https://doi.org/10.5194/egusphere-2025-6347
Preprint. Discussion started: 15 January 2026

Southern Ocean biological pump over the last glacial cycle from new diatom transfer functions

Mathieu Rembauville[1], Sylvain Pichat[1,2]

[1]Univ. Lyon, ENS de Lyon, Université Lyon 1, CNRS, UMR 5276 LGL-TPE, 69364, Lyon, France

[2]Climate Geochemistry Department, Max Planck Institute for Chemistry, Mainz, Germany

Correspondance to : Mathieu Rembauville (mathieu.rembauville@ens-lyon.fr)

Abstract. We present new transfer functions to reconstruct deep ocean (~1000 m) particulate organic carbon (POC) flux and particulate inorganic to organic carbon export ratio (PIC:POC) from diatom assemblage in the Southern Ocean. The transfer functions were calibrated with modern sediment trap data covering the three ocean sectors of the Southern Ocean. They were then applied to ten sediment cores located in the Antarctic Zone (AZ) in the three Southern Ocean basins. The diatom community appears to catch efficiently the ecosystem structure that sets the magnitude and stoichiometry of the export fluxes with root mean square errors of the prediction ranging 17-19.6 % depending on the transfer function. A consistent climatic signal is observed in all sediment cores : the reconstructed deep-ocean POC export is higher during glacial than interglacial periods. The PIC:POC ratio is low during glacial periods and increases quickly after glacial maxima. These two signals suggest that both the increase in the biological carbon pump and the decrease in the carbonate counter-pump in the AZ during glacial periods could have contributed to the decrease in atmospheric pCO_2. The reconstructed POC export is consistent with previously published diatom-bound $\delta^{15}N$ and total organic carbon content but differs from elemental Ba/Fe ratio, hinting Ba potential preservation issues in Southern Ocean sediments. At the global Southern Ocean scale, the deep-ocean POC export flux decreases by 50 % and the PIC:POC export ratio increases by 17 % during the last deglaciation. While the glacial/interglacial POC flux change is comparable in the three SO sectors, the PIC:POC change is weaker in the Pacific, suggesting a distinctive response of the calcifying plankton community to glacial conditions in this sector. We suggest two mechanisms likely to increase the biological pump efficiency during glacial periods : 1) iron fertilization increasing primary production combined with diatom spore formation that increases export efficiency, and 2) a northward extension of sea ice edge supporting a greater zooplankton-mediated export that increases transfer efficiency. These new transfer functions quantitatively support a glacial iron fertilization effect in the AZ, contrasting with the view of a fertilization effect restricted to the Subantarctic Zone.

https://doi.org/10.5194/egusphere-2025-6347
Preprint. Discussion started: 15 January 2026

1 Introduction

The Southern Ocean (SO) is the largest ocean on Earth, connecting the three other oceanic basins and providing nutrients to the global ocean thermocline (Sarmiento et al., 2004). The majority of the modern SO waters are qualified as "high nutrient, low chlorophyll" (HNLC) due phytoplankton growth limitation by micronutrients such as iron (de Baar et al., 1990). The macronutrient availability and leakage to lower latitudes suggests that the vertical transfer of particulate organic matter from the surface to the deep ocean, i.e. the biological pump, is inefficient (Sarmiento and Toggweiler, 1984; Sigman et al., 2010). Ice cores revealed that during the Last Glacial Maximum (LGM, 19 000 – 23 000 years ago) atmospheric pCO_2 was ~90 ppmv lower than preindustrial levels (Petit et al., 1999). Physical processes have been invoked to explain the role of the SO in lowering LGM atmospheric pCO_2 such as changes in vertical stratification and dense water formation (Toggweiler, 1999; Sigman et al., 2010) or changes in sea-ice extent (Stephens and Keeling, 2000; Stein et al., 2020). However, these physical processes appear insufficient to explain the entire LGM pCO_2 decrease (Archer et al., 2000).

Another mechanism has been proposed to lower the atmospheric pCO_2 during glacial periods: an increased iron supply to the HNLC zones of the SO via increased atmospheric dust flux. The larger input of this essential and limiting micronutrient would have led to an increase in macronutrient utilization and a more efficient biological pump (Martin, 1990; Kohfeld et al., 2005; Jaccard et al., 2013; Martínez-García et al., 2014; Shoenfelt et al., 2018). Numerical models suggest that a stronger biological pump during the LGM could account for a 30 – 50 ppmv decrease in atmospheric pCO_2 (Bopp et al., 2003; Tagliabue et al., 2009; Lambert et al., 2015; Yamamoto et al., 2019). The first reconstruction of the biological pump during the LGM considered that the entire SO was fertilized, resulting in higher nutrient utilization and subsequent export production in both the Subantarctic Zone (SAZ) and the Antarctic Zone (AZ) south of the polar front (Moore et al., 2000). However, additional export proxies suggested a latitudinal response of the SO to glacial conditions : an increased biological pump in the SAZ due to dust-driven fertilization of phytoplankton growth, but a weaker biological pump in the AZ due to higher stratification and lower micronutrient enrichment (François et al., 1997; Jaccard et al., 2013; Sigman et al., 2021). These results were established based on different production and/or export proxies applied to different latitudinal sectors of the SO.

An additional biological mechanism likely to affect atmospheric CO_2 is the carbonate counter-pump, i.e. the release of CO_2 associated with particulate inorganic carbon (PIC) precipitation by calcifying organisms (Frankignoulle et al., 1994). This CO_2 source lowers the effect of CO_2 sequestration into particulate organic carbon (POC) caused by the biological pump. Therefore, the PIC:POC ratio of the exported particles is an estimate of the carbonate counter-pump intensity (Sarmiento et al., 2002). An increased carbonate counter-pump was suggested during the last deglaciation in the SAZ of the SO Pacific sector (Duchamp-Alphonse et al., 2018) as well as during warm periods such as MIS 3 in the polar frontal zone (PFZ) of the Indian sector (Brandon et al., 2022) and MIS 11 in the SAZ of the Pacific sector (Anderson et al., 2024).

Several proxies have been proposed to reconstruct the biological pump in the past (Kohfeld et al., 2005). Organic carbon export has been derived from sediment organic carbon (Corg) concentration rate normalized to ^{230}Th, i.e. the true vertical Corg flux (Francois et al., 2004; Thöle et al., 2019) or from barite accumulation rate, i.e. the true vertical biogenic barite flux, with biogenic barite or barium (Ba) excess defined as the difference between total Ba and Ba of lithogenic origin (Dymond et al., 1992; François et al., 1997; Hernandez-Sanchez et al., 2011). Nutrient utilization in the surface ocean has been estimated from stable isotopes such as $\delta^{15}N$ (Martínez-García et al., 2014; Studer et al., 2015, 2018; Wang et al., 2017)

https://doi.org/10.5194/egusphere-2025-6347
Preprint. Discussion started: 15 January 2026

and $\delta^{13}C$ (Vollmer et al., 2022). Although these approaches provided key information on the relative changes in the biological pump during glacial/interglacial cycles or millennial events, they do not reconstruct absolute carbon fluxes. Quantitative estimates of the biological pump and carbonate counter-pump are needed to understand the impact of oceanic biological processes on the glacial/interglacial atmospheric CO_2 changes. Past oceanic conditions are commonly reconstructed quantitatively using transfer functions : a statistical relationship between oceanic variables and the community structure of a microfossil record (Juggins, 2013). The first transfer function was built to reconstruct past ocean temperature and salinity from pelagic foraminifer assemblage using factorial analysis followed by multiple linear regressions (Imbrie and Kipp, 1971). The modern analog technique was then proposed, calculating the foraminifer assemblage dissimilarity between down-core samples and a reference sample of known oceanographic conditions (Hutson, 1980). Both techniques were extended to siliceous microfossils to reconstruct glacial Southern Ocean temperature and sea ice extent (Gersonde et al., 2005), and further combined with chemical proxies to map the global ocean LGM temperature (Waelbroeck et al., 2009). More recently, partial least square regression (PLSR), was used to reconstruct past sea surface temperature from diatom assemblages in the North Atlantic (Berner et al., 2008) and the Southern Ocean (Esper and Gersonde, 2014).

Diatom community structure has a strong influence on the biological pump intensity and stoichiometry at global scale (Tréguer et al., 2018). Sediment trap studies in the Southern Ocean have provided a quantitative link between diatom species and POC or biogenic silica fluxes (Salter et al., 2012; Rembauville et al., 2015; Rigual-Hernández et al., 2015a). In this study, we develop new transfer functions based on diatom community structure to reconstruct the deep-ocean POC flux and PIC:POC export ratio. These transfer functions are calibrated on modern Southern Ocean sediment trap data and then applied to sediment cores in order to quantitatively reconstruct the variations in the intensity of the biological pump and the carbonate counter-pump over the last glacial cycle.

2 Materials and method

2.1 Sediment traps and sediment cores data

We compiled sediment trap records from the Southern Ocean (south of 40 °S) for which POC, PIC and diatom export fluxes were reported. We excluded 1) records in which only few diatom species were qualitatively or semi-quantitatively enumerated (e.g. Abelmann and Gersonde, 1991; Fischer et al., 2002; Salter et al., 2012), 2) sediment traps located at less than 100 m above the seafloor as these are prone to sediment resuspension (e.g. Pudsey and King, 1997), and 3) upper ocean sediment traps deployed over shallow island plateaus as these are not representative of deep-ocean fluxes (Rembauville et al., 2015). Eventually, the dataset contains 11 sediment trap locations from the SAZ to the seasonal ice zone (SIZ) in the Atlantic, Indian and Pacific sectors of the SO, at a mean depth of 1250 m (range 830 - 2000 m b.s.l.), with total collection duration from 321 to 2 328 days (Table 1, Fig. 1). These sediment trap data reflect the ecological and biogeochemical gradient from the SAZ to the SIZ. The dataset includes warm water species, ice-related species as well as bloom-forming species and covers a wide range of biogeochemical fluxes magnitude and stoichiometry from iron-limited to naturally iron-fertilized sites (Fig. 2). All the traps are located above the calcite compensation depth of ~3000 to 4000 m in the Southern Ocean (Feely et al., 2004). The dataset represents a total number of 256 samples, however the samples distribution is not equal across the sediment trap locations (Table 1). In order to avoid the geographical bias in the transfer function due to the

https://doi.org/10.5194/egusphere-2025-6347
Preprint. Discussion started: 15 January 2026

unequal sampling effort, seasonal averages of sediment trap data where calculated for spring (September to November), summer (December to February), autumn (March to May) and winter (June to August). Thereby each sediment trap location has the same weight in the transfer functions calibration. The deployment depths are located in the deep mesopelagic ocean where the PIC and POC flux attenuation with depth is low, most of the flux attenuation occurring in the upper mesopelagic ocean (Martin et al., 1987; Marsay et al., 2015). The depth-dependent POC and PIC flux attenuation factor is highly variable at short time and space scales (Marsay et al., 2015; Henson et al., 2023; Williams et al., 2025) and cannot be addressed individually for every location and season. For this reason, the biogeochemical fluxes were not normalized to a standard depth. We consider the fluxes as representative of the deep ocean (~1000 to 2000 m) where carbon can be sequestrated over climate-relevant timescales (Siegel et al., 2021).

To test and apply transfer functions, we also compiled Southern Ocean sediment cores records in which detailed diatom counts were previously published (Table 2). These are located in three of the four zones encompassed by the sediment traps (Fig. 1) and cover the last 15 ka to 150 ka. All the sediment core diatom data, the associated geochemical variables and the age models were accessed at www.pangea.de.

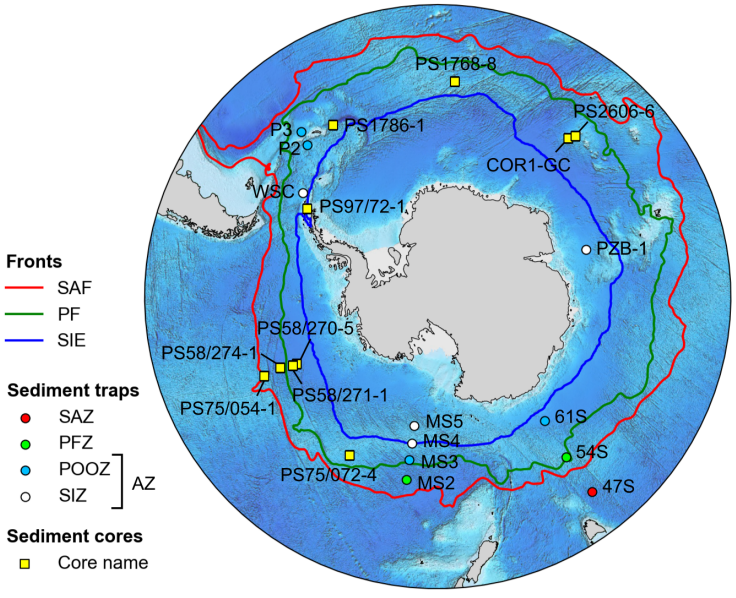

Figure 1. Location of the sediment traps (see Table 1 for details) and sediment cores (see Table 2 for details) used in this study. The subantarctic (SAF) and polar (PF) fronts are defined from dynamic topography (Park et al., 2019). Sea ice edge (SIE) refers to the September sea ice edge climatology (National Snow and Ice Data Center). SAZ: subantarctic zone, PFZ: polar frontal zone, POOZ: permanently open ocean zone, SIZ: seasonal ice zone, AZ: antarctic zone.

https://doi.org/10.5194/egusphere-2025-6347
Preprint. Discussion started: 15 January 2026

Table 1. Sediment trap records used to calibrate the diatom transfer functions. They are sorted along north-south transects when existing. See Fig. 1 for locations.

Site	Zone	Lon. (°E)	Lat. (°N)	Depth (m)	Start date	Stop date	Duration (days)	Samples	Reference
MS-2	PFZ	-170.17	-56.9	982	1996-11-28	1998-01-27	425	20	Honjo et al., 2000; Grigorov et al., 2014
MS-3	POOZ	-170.05	-60.28	1003	1996-11-28	1998-01-27	425	12	Honjo et al., 2000; Grigorov et al., 2014
MS-4	SIZ	-169.9	-63.15	1031	1996-11-28	1998-01-27	425	13	Honjo et al., 2000; Grigorov et al., 2014
MS-5	SIZ	-169.67	-66.17	937	1996-11-28	1998-01-27	425	10	Honjo et al., 2000; Grigorov et al., 2014
47S	SAZ	142.07	-46.77	1060	1999-07-31	2001-10-13	805	29	Rigual-Hernández et al., 2015a
54S	PFZ	141.75	-53.75	830	1997-09-26	2004-02-10	2328	108	Rigual-Hernández et al., 2015b
61S	POOZ	139.9	-60.75	2000	2001-11-30	2002-09-29	303	20	Rigual-Hernández et al., 2015b
P2	POOZ	-41.12	-55.02	1500	2012-01-15	2012-12-01	321	9	Rembauville et al., 2016
P3	POOZ	-40.13	-52.72	2000	2012-01-15	2012-12-01	321	11	Rembauville et al., 2016
PZB-1	SIZ	72.98	-62.48	1400	1998-12-30	1999-12-13	348	13	Rigual-Hernández et al., 2019
WSC	SIZ	-53	-60	1000	2012-03-01	2013-02-01	337	11	Zúñiga et al., 2021

Table 2. Sediment cores used to apply the diatom transfer functions.

Core	Zone	Lon. (°E)	Lat. (°N)	Depth (m)	Diatom counts	Age model
PS97/72-1	SIZ	-56.06	-62.01	1993	Vorrath et al., 2023	Vorrath et al., 2023
PS1768-8	POOZ	4.48	-52.59	3270	Zielinski et al., 1998	Frank and Mackensen, 2002
PS1786-1	POOZ	-31.72	-54.92	5862	Jacot Des Combes et al., 2008	Jacot Des Combes et al., 2008
COR1-GC	POOZ	39.77	-54.27	2834	Orme et al., 2020	Orme et al., 2020
PS2606-6	POOZ	40.8	-53.23	2545	Jacot Des Combes et al., 2008	Jacot Des Combes et al., 2008 extended by Civel-Mazens et al., 2024
PS58/270-5	POOZ	-116.12	-62.03	4981	Benz et al., 2016	Benz et al., 2016
PS58/271-1	POOZ	-116.05	-61.24	5214	Esper and Gersonde, 2014	Benz et al., 2016
PS58/274-1	PFZ	-114.89	-59.21	5138	Benz et al., 2016	Benz et al., 2016
PS75/054-1	POOZ	-115.13	-56.15	4113	Benz et al., 2016	Benz et al., 2016
PS75/072-4	PFZ	-151.22	-57.56	3099	Benz et al., 2016	Benz et al., 2016

https://doi.org/10.5194/egusphere-2025-6347
Preprint. Discussion started: 15 January 2026

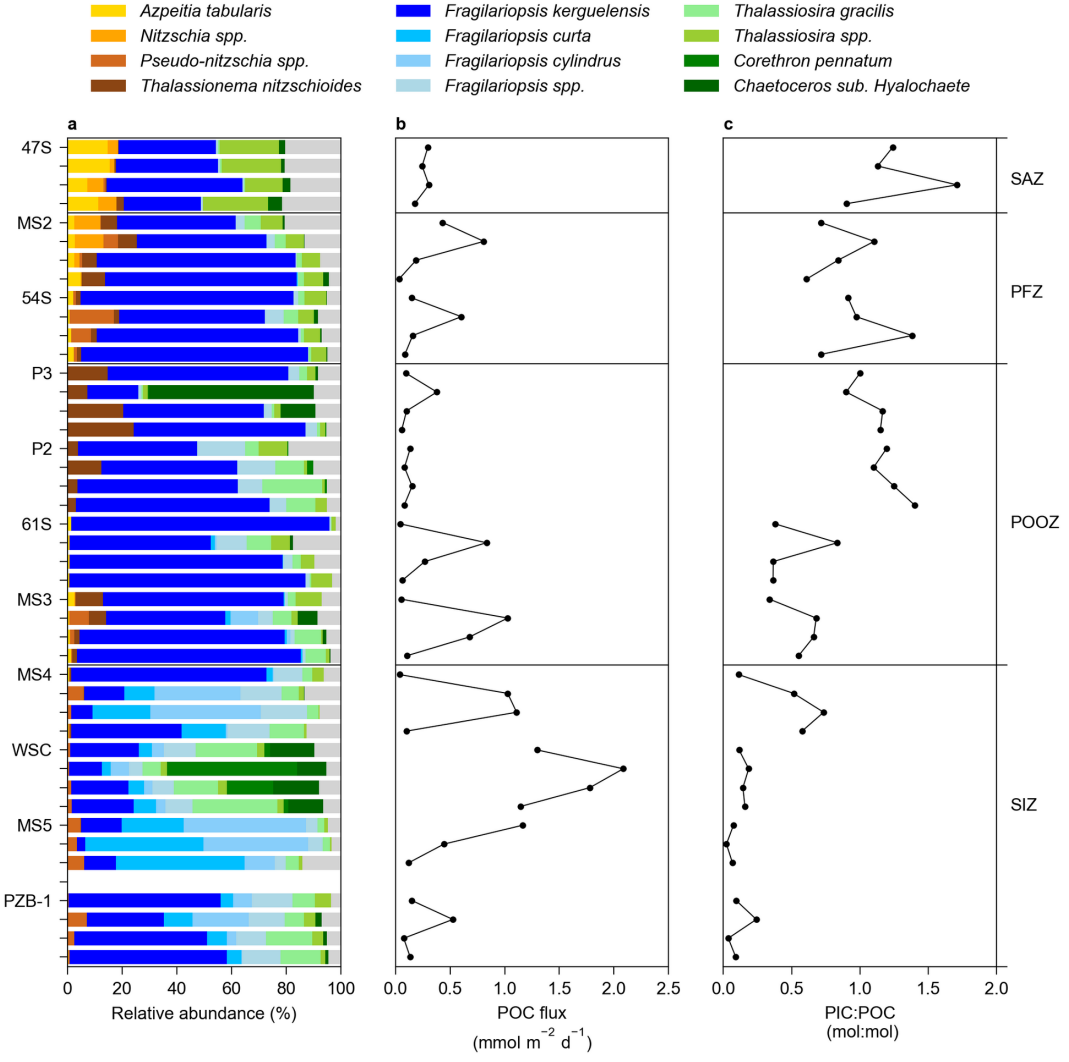

119 **Figure 2.** Seasonal averages of diatom species and biogeochemical fluxes from the sediment traps (see Fig. 1 and Table 1
120 for details). Sediment traps are sorted by location form north (top) to south (bottom) and for each sediment trap by season
121 from spring (top) to winter (bottom). a) Relative abundance of the main diatom species (grey bars represent other species
122 not reported in the legend). b) Particulate organic carbon (POC) flux. c) Particulate inorganic to organic carbon (PIC:POC)
123 export ratio. Winter data are not available for trap MS5.

https://doi.org/10.5194/egusphere-2025-6347
Preprint. Discussion started: 15 January 2026

2.2 Diatom datasets homogenization

Diatom identifications reported in the sediment trap data are based on different sample preparation methods : some studies used a micropaleontological technique to oxidize organic matter (e.g. Grigorov et al., 2014; Rigual-Hernández et al., 2015) whereas others used a biological technique to differentiate full and empty frustules (Rembauville et al., 2016b). When the latter method was applied, the sum of empty and full frustule flux was used. The sediment trap data and the sediment core data contains 128 and 90 diatom species/taxa groups, respectively. Diatom species names were homogenized and updated to currently accepted taxonomic entities following Algeabase recommendations (www.algeabase.org) to a total number of 154 species/taxa group (see the Supplementary Information for the updated names and the full species list). As some sediment core records do not differentiate the vegetative stages from the resting spores (e.g. Jacot Des Combes et al., 2008; Orme et al., 2020), we chose to merge 1) *Chaetoceros* resting spores were with *Chaetoceros* subgenus *Hyalochaete* vegetative stages, 2) *Eucampia antarctica* resting spores with *Eucampia antarctica* vegetative stages and 3) *Thalassiosira antarctica* resting spores with *Thalassiosira antarctica* vegetative stages.

For transfer functions calibration, only the species present in both the sediment trap and sediment core dataset were selected, i.e. 64 species/taxa groups (Fig. 3). In order to avoid the bias associated with rare species, a filter was applied to select species occurring with at least a relative abundance of 0.1 % in both datasets (Esper and Gersonde, 2014). This final step resulted in a list of 22 informative species. Based on those, relative abundances were recalculated for the two selected datasets before using the the data to calibrate the transfer functions.

https://doi.org/10.5194/egusphere-2025-6347
Preprint. Discussion started: 15 January 2026

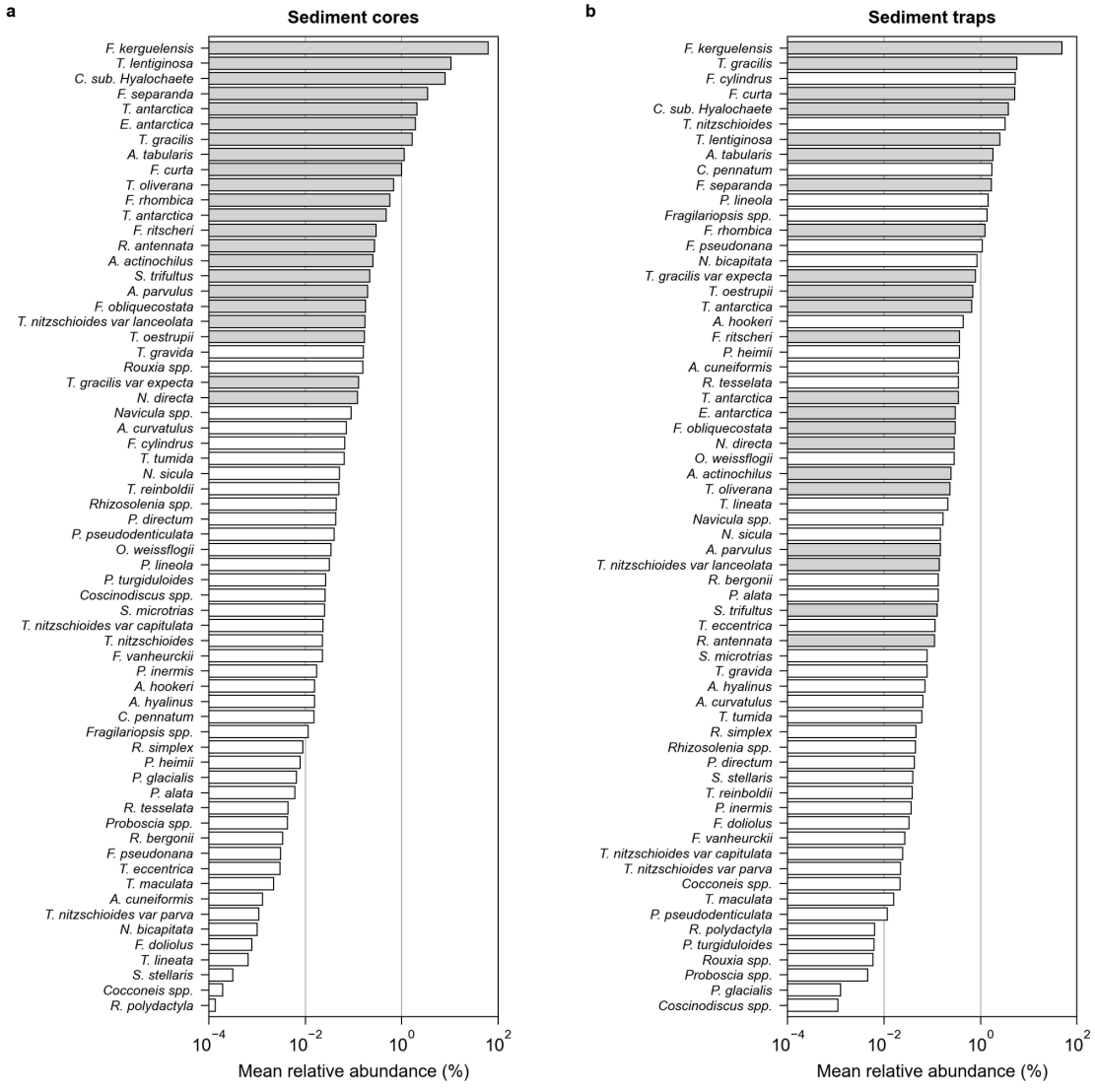

141 **Figure 3.** Mean relative abundance of diatom species reported in the sediment core and the sediment trap datasets. Grey
142 bars represent species with a mean relative abundance higher than 0.1 % in both datasets.

https://doi.org/10.5194/egusphere-2025-6347
Preprint. Discussion started: 15 January 2026

2.3 Transfer functions development

Previous studies reported the direct quantitative link between plankton community structure and carbon export fluxes (e.g. Rembauville et al., 2015, 2016a). Here, the diatom community composition is considered as an integrator of the ecosystem structure that is the ultimate driver of the magnitude and stoichiometry of the export fluxes. The seasonal sediment trap dataset was used to calibrate transfer functions in order to reconstruct the deep-ocean POC flux and PIC:POC export ratio based on the diatom diversity. Three transfer functions were built : multiple linear regression (MLR), partial lest square regression (PLSR) and gradient boosting regression (GBR) using log-transformed and standardized diatom relative abundance (mean subtracted, divided by standard deviation).

For MLR, diatom relative abundances were transformed by factorial analysis with varimax rotation following the method developed by Imbrie and Kipp (1971). A scree test was used to identify significant factors associated with an eigenvalue > 1 (Cattell, 1966 ; Fig. S1), resulting in four informative factors used to build the linear model. While in the original method proposed by Imbrie and Kipp (1971), factors interactions and squared terms were added to the regression model, given the limited amount of data in our approach, we only used the linear combination of the four factors in order to avoid overfitting of multiple terms that artificially increases the model coefficient of determination (R^2) at the expense of higher error in the prediction from new data, i.e. the bias-variance tradeoff.

PLSR is a statistical method that builds a linear model between multivariate data by projecting the original matrices in a new space of maximum covariance. Dimensionality reduction restrains the weight of co-occurring species, making this approach useful to link ecological data with chemical fluxes (Rembauville et al., 2015, 2017; Salter, 2018; Blain et al., 2022). PLSR was already identified as an efficient method to build transfer functions from diatom assemblages in conjunction with MLR (Esper and Gersonde, 2014). The choice of the number of components to keep in the PLSR is another case of bias-variance tradeoff. To identify the significant components, the variance explained by the PLSR components was compared to a broken stick model, i.e. a null model in which decreasing variance is evenly distributed among components (Jackson, 1993). The first two components explained more variance than the null model and were thus selected for the PLSR calibration (Fig. S2).

GBR is a machine learning technique that builds a series of decision trees, each aimed at correcting the errors of the previous ones (Friedman, 2001). It produces a final model from an ensemble of weak predictive models. Each decision tree can integrate non-linear relationships and interactions that are not considered in linear modeling frameworks, making GBR a useful tool for the study of complex communities (Maloney et al., 2012). Two key parameters must be set when building a gradient boosting regressor : 1) tree depth, i.e. the number of nodes in the tree and 2) the number of estimators, i.e. the number of boosting stages that will be performed. These two parameters were selected using bootstrapping. The dataset was split into a learning set containing 2/3 of the data and a test set with the remaining 1/3 of the data. The root mean squared error (RMSE) of the prediction was calculated for 10 000 permutations of train/test sets and performed with different combinations of tree depth and number of estimators. The combination minimizing the RMSE of the prediction for both the POC flux and the PIC:POC ratio was a tree depth of 2 with 30 estimators (Fig. S3).

The precisions of the MLR, PLSR and GBR transfer functions were calculated by bootstrapping using the same conditions as above (a learning set with 2/3 of the data, a test set with the remaining of the data and 10 000 permutations).

https://doi.org/10.5194/egusphere-2025-6347
Preprint. Discussion started: 15 January 2026

2.4. Application of the transfer functions to sediment cores

The three transfer functions were applied to each of the sediment cores described in section 2.1 in order to quantitatively reconstruct the biological pump and carbonate counter-pumps over the last 15 to 150 ka in the various sectors of the Southern Ocean. Because sediment core samples integrate a pluriannual signal, the reconstructed POC fluxes were converted from seasonal to annual averages using a mean year duration of 365.25 days. All the data analyses were performed with Python and statistical models were implemented with the scikit-learn package (Pedregosa et al., 2011).

3 Results

3.1 Diatom species association with POC flux and PIC:POC ratio

The species scores on factors from the factor analysis used in the MLR prediction are presented in Table 3. Factor 1 is characterized by warm-water species typical of the SAZ (*Azpeitia tabularis*, *Shionodiscus trifultus*) and small *Thalassiosira* species such as *Thalassiosira oestrupii*, together with the giant mat-forming species *Thalassiothrix antarctica*. Factor 2 is associated with ice-related species *Fragilariopsis curta* together with other small *Fragilariopsis* species of the SIZ. Factor 3 contains bloom-forming species often observed as resting spore in naturally iron-fertilized locations (*Chaetoceros* subgenus *Hyalochaete*, *Eucampia antarctica*, *Thalassiosira antarctica*) together with background species generally found in the POOZ (*Actinocyclus actinochilus*, *Fragilariopsis obliquecostata*). Factor 4 contains rare and large species sometimes associated with the PFZ such as *Asteromphalus parvulus* and *Rhizosolenia antennata*.

The MLR coefficients are provided in Table 4. The strongest positive correlation with POC flux is observed for factor 2 (ice-related species) and moderate positive correlations for factors 3 (spores and bloom-forming species) and 4 (large PFZ species). A negative correlation is observed for factor 1 (SAZ and warm-water species). For the PIC:POC ratio, a positive correlation is observed with factor 1 (SAZ warm-water species) whereas all the other factors are negatively correlated. The two MLR models for both POC flux and PIC:POC ratio are highly significant (global Fisher test, $p < 0.01$).

https://doi.org/10.5194/egusphere-2025-6347
Preprint. Discussion started: 15 January 2026

Table 3. Diatom scores on factors from the factor analysis with varimax rotation used in the MLR transfer function. Major values are highlighted in bold.

Species	Factor 1	Factor 2	Factor 3	Factor 4
Actinocyclus actinochilus	-0.15	0.34	**0.77**	0.05
Asteromphalus parvulus	-0.19	0.03	-0.14	**0.48**
Azpeitia tabularis	**0.94**	-0.22	-0.15	-0.10
Chaetoceros sub. *Hyalochaete*	0.13	-0.07	**0.83**	-0.05
Eucampia antarctica	-0.39	-0.51	**0.47**	-0.18
Fragilariopsis curta	-0.22	**0.81**	0.14	0.17
Fragilariopsis kerguelensis	0.09	-0.53	-0.37	0.02
Fragilariopsis obliquecostata	-0.17	0.39	**0.75**	0.10
Fragilariopsis rhombica	-0.13	**0.58**	0.38	0.53
Fragilariopsis ritscheri	-0.07	**0.71**	-0.09	0.54
Fragilariopsis separanda	-0.20	**0.63**	0.06	0.27
Navicula directa	-0.16	-0.52	0.00	0.17
Rhizosolenia antennata	0.12	0.04	0.01	**0.63**
Shionodiscus trifultus	**0.73**	-0.05	0.06	-0.01
Thalassionema nitzschioides var *lanceolata*	0.31	-0.46	-0.04	0.15
Thalassiosira antarctica	-0.27	-0.05	**0.79**	-0.23
Thalassiosira gracilis	-0.44	**0.51**	0.20	-0.12
Thalassiosira gracilis var *expecta*	-0.05	0.08	0.02	**0.99**
Thalassiosira lentiginosa	0.25	-0.12	-0.19	0.21
Thalassiosira oestrupii	**0.88**	-0.04	-0.12	-0.18
Thalassiosira oliverana	0.10	-0.31	-0.28	**0.34**
Thalassiothrix antarctica	**0.84**	-0.09	-0.17	0.04

Table 4. Coefficients of the multiple linear regression performed on the four factors from the factorial analysis of diatom relative abundance (log-transformed and standardized data).

Response variable	Intercept	Factor 1	Factor 2	Factor 3	Factor 4	Model *p*-value
POC (mmol/m^2/d^{-1})	0.439	-0.136	0.330	0.046	0.066	4 .10^{-4}
PIC:POC (mol:mol)	0.669	0.033	-0.149	-0.028	-0.224	2 .10^{-6}

https://doi.org/10.5194/egusphere-2025-6347
Preprint. Discussion started: 15 January 2026

3.2 Transfer functions accuracy

Transfer functions coefficient of determination (R^2) varies depending on the method and the response variable considered (Fig. 4). The MLR, despite providing valuable information on the association of diatoms groups with export fluxes, has low R^2 values for both POC flux (0.41) and the PIC:POC ratio (0.56). The PLSR increases the prediction quality with R^2 reaching 0.68 for POC flux and 0.64 for the PIC:POC ratio. The GBR provided the highest R^2 for both the POC flux and the PIC:POC ratio (0.94 and 0.95, respectively). A better estimation of transfer function accuracy is provided by the calculation of the RMSE from bootstrapping (Fig. 5). For POC flux reconstruction, the highest mean error is associated with MLR (19.6 %), also characterized by a high error dispersion reaching up to 40 % while PLSR has the lowest mean error (17 %), associated with a low error dispersion. For the PIC:POC ratio, GBR has the lowest mean error (17.8 %) whereas MLR provides the lowest error dispersion.

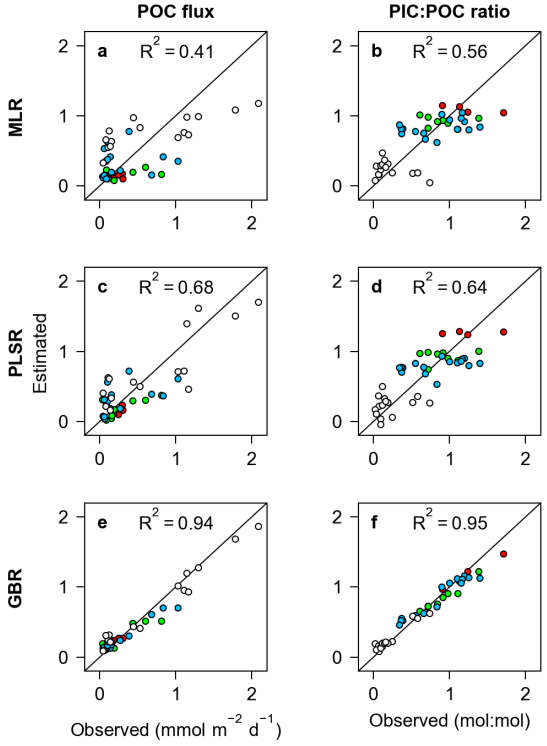

Figure 4. Biogeochemical fluxes (POC flux : particulate organic carbon flux, PIC:POC ratio :particulate inorganic to organic carbon ratio) estimated from the three transfer functions (MLR: multiple linear regression, PLSR: partial least squares regression, GBR: gradient boosting regression). Black line represents the 1:1 relationship, color code defines the four Southern Ocean zones as in Fig. 1.

https://doi.org/10.5194/egusphere-2025-6347
Preprint. Discussion started: 15 January 2026

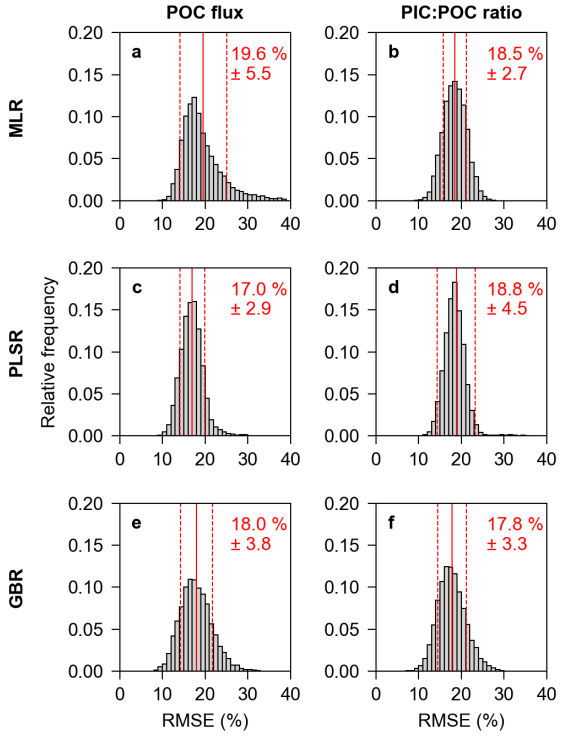

Figure 5. Root mean square error (RMSE) of the prediction for each transfer function and the two variables (POC flux and PIC:POC ratio) derived from bootstrapping (10 000 iterations). The red continuous and dotted lines show respectively the mean and one standard deviation around the mean.

3.3 Reconstructed deep-ocean fluxes over the last glacial cycle

The three transfer functions provide convergent predictions with clear glacial/interglacial changes for the 10 sediment cores used in this study (Fig. 6). Reconstructed deep-ocean POC fluxes are higher during marine isotopic stages (MIS) 2, 4 and 6 associated with colder conditions and decrease during the Holocene and MIS 5 interglacials. An abrupt increase in PIC:POC ratio is observed during both deglaciations at the end of MIS 2 and MIS 6. These signals are observed in the three sectors of the Southern Ocean : Atlantic (Fig. 6b, c), Indian (Fig. 6e) and Pacific (Fig. 6f, g, h, i, j). The two cores with a high temporal resolution show similar trends during the Antarctic Cold Reversal (ACR) : a small increase in POC flux whereas the PIC:POC ratio slightly decreases (Fig. 6a, d). In the POOZ, throughout the Holocene, POC flux are lower at the beginning of the Holocene, followed by a gradual increase toward the modern area (Fig. 6b, c, d, e, g, h). This trend is not observed in the coastal SIZ where the POC flux remains low throughout the Holocene (Fig. 6a).

https://doi.org/10.5194/egusphere-2025-6347
Preprint. Discussion started: 15 January 2026

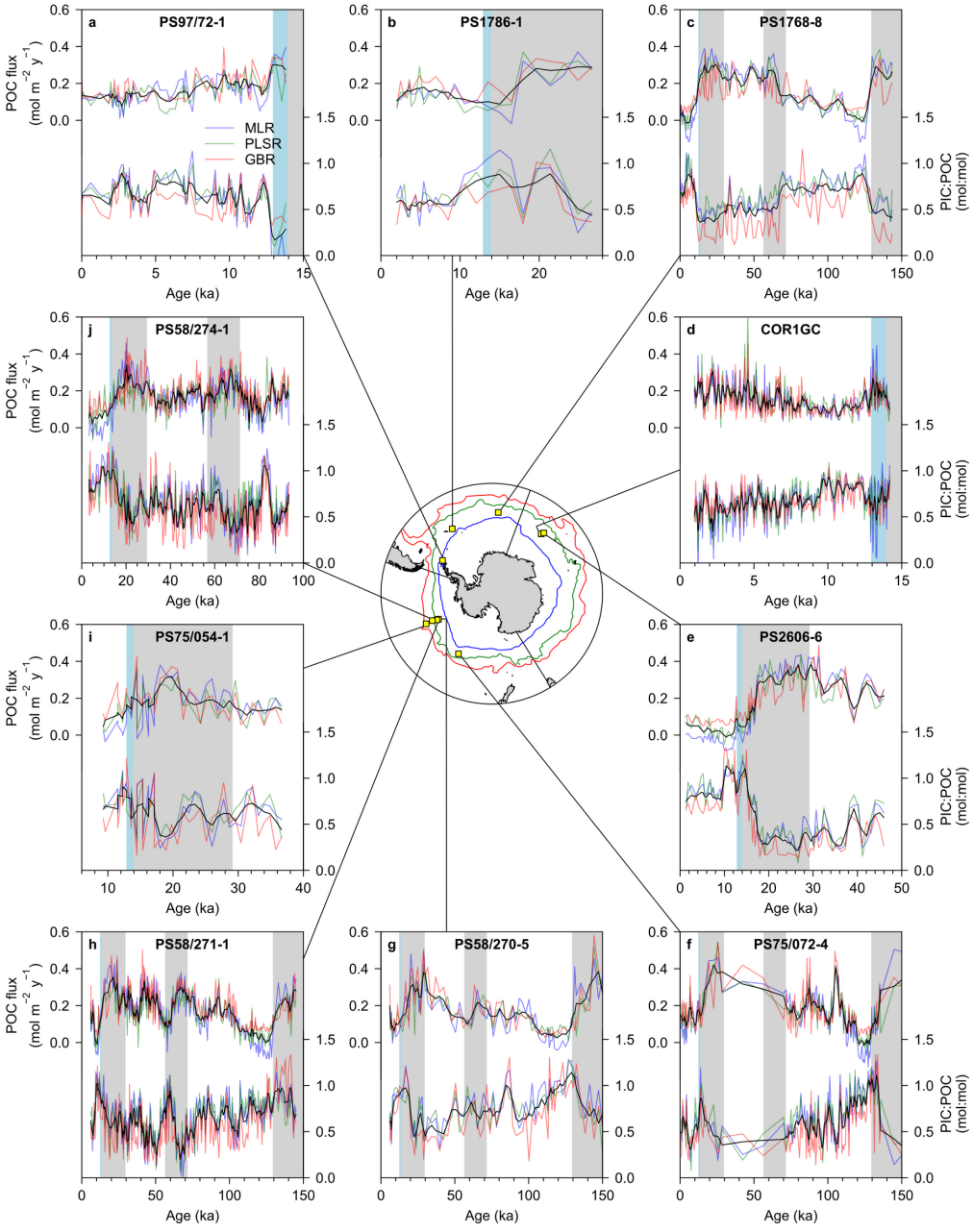

231 **Figure 6.** Application of the three transfer functions to sediment cores (blue: MLR - multiple linear regression, green: PLSR
232 - partial least square regression, red: GBR - gradient boosting regression). Black lines represent the three transfer functions
233 moving average. Vertical grey bars indicate marine isotopic stages (MIS) 2, 4 and 6. The vertical blue bar indicates the
234 Antarctic Cold Reversal. Fronts represented in the central map are the same as in Fig. 1.

https://doi.org/10.5194/egusphere-2025-6347
Preprint. Discussion started: 15 January 2026

When focusing on the deep open-ocean, i.e. excluding the coastal SIZ core PS97/72-1, the three transfer functions show that the POC flux is significantly higher during MIS 2 compared to the Holocene in the three Southern Ocean basins (Fig. 7a). The MIS 2 mean global Southern Ocean POC flux is 0.25 ± 0.09 mol m^{-2} y^{-1} (mean ± standard deviation), ca. 1.5 times the average modern mean sediment trap value, however remaining within the range of the observed modern values. Over the Holocene, the mean SO POC flux is 0.12 ± 0.08 mol m^{-2} y^{-1} which represents 50 % of the MIS 2 flux. This Holocene mean value also overlaps with that of modern sediment trap fluxes. Changes in the PIC:POC export ratio appear more basin-specific (Fig. 7b). In the Atlantic and Indian sectors, the mean PIC:POC ratio increases from 0.52 to 0.68 between MIS 2 and the Holocene whereas in the Pacific sector, the increase is only weakly significant from 0.61 to 0.68. In the three sectors, the reconstructed Holocene values are close to that of the modern sediment traps (0.65). The global Southern Ocean mean PIC:POC export ratio significantly increases from 0.58 to 0.68 (+17 %) from MIS 2 to the Holocene. The difference in the PIC:POC export ratio between MIS 2 and the modern sediment trap data is +13 %.

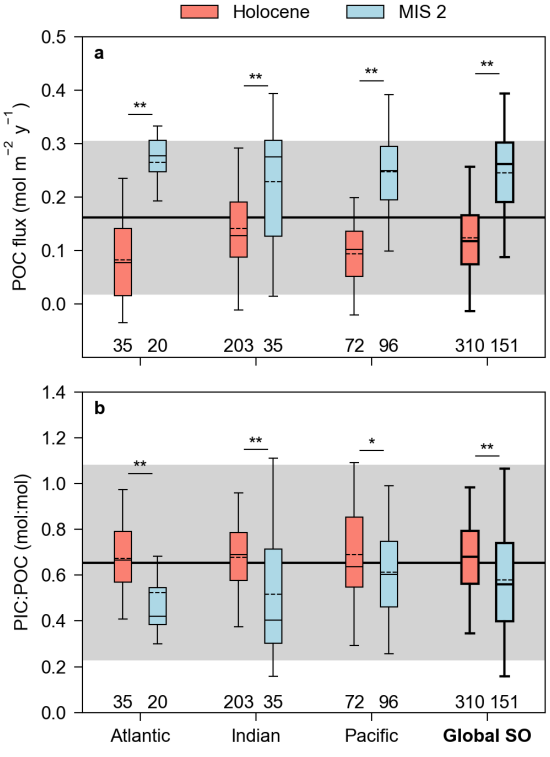

Figure 7. Comparison of the Holocene and MIS 2 reconstructed export fluxes pooling the three transfer functions. a) deep-ocean POC fluxes and b) deep-ocean PIC:POC export ratio in the three sectors of the Southern Ocean (SO) and for the global SO. In each boxplot, the median and the mean are represented by continuous and dotted lines, respectively. Asterisks represent significantly different samples (Mann-Whitney U test, * : $p < 0.05$, ** : $p < 0.01$). Samples sizes are given at the bottom of each panel. The horizontal black line and grey area represent the mean ± standard deviation of the modern ocean sediment trap values.

https://doi.org/10.5194/egusphere-2025-6347
Preprint. Discussion started: 15 January 2026

4 Discussion

4.1 Validity of diatom communities to reconstruct the ocean carbon pumps

The relative abundance of diatom species shows noticeable differences in the sediment trap and sediment core data. Small ubiquitous species that are abundant in the sediment traps such as *Pseudo-nitzschia lineola* or *Nitzschia bicapitata* are rare in the sediment cores. It is also the case for larger species such as *Corethron pennatum* and *Asteromphalus hookeri*. The slope of the rarefaction curse is steeper in the sediment core dataset when compared to the sediment trap data, with the most abundant species in the cores characterized by a heavily silicified frustule (e. g. *Fragilariopsis* and large *Thalassoisira* species). These results confirm previous observations of selective dissolution of lightly silicified species in the deep ocean below the sediment traps depth (Warnock and Krueger, 2020; Ran et al., 2024). Hence, the selection of informative species in both datasets is a critical preliminary step before calibrating the transfer functions. The resulting rather small number of in formative species (here 22) is due to the merging of the sediment trap and sediment core datasets in which the most abundant species are different. This number is however only slightly lower than those in studies based on core-top diatom communities, typically 25 to 29 species (Imbrie and Kipp, 1971; Crosta et al., 1998; Esper and Gersonde, 2014).

The convergence of the three transfer functions in every sediment core supports the reliability of the reconstructed signals. The MLR is associated with higher error dispersion, potentially leading to negative values for periods of very low POC flux. In this sense the PLSR and GBR appear as better estimators of POC export that are less prone to extrapolation during periods of low or high flux. Globally the RMSE of the new transfer functions proposed here (17-19.6 %) is higher than those of previously published diatom-based proxies: 5-6 % for summer the sea surface temperature (Esper and Gersonde, 2014) and below 5 % for sea-ice cover (Crosta et al., 1998). The lower accuracy of the new proxies presented in this study can be attributed to the restricted amount of sediment trap data available for the calibration (43 seasonal averages) which is much lower than the abundant core-top data used in previously published diatom-based proxies (100 to 450 samples, Crosta et al., 1998; Esper and Gersonde, 2014). Despite this relatively high RMSE, the reconstructed POC flux and PIC:POC ratio remain in the range of observed values in the SO modern ocean which supports the consistency of the reconstructed values.

The factorial analysis clusters diatom species into ecologically consistent groups, highlighting hydrological zones of the Southern Ocean as the most structuring factor of diatom biogeography as previously reported (Crosta et al., 1998; Esper and Gersonde, 2014). The deep-ocean POC flux is positively correlated with ice-related species as well as with bloom-forming and spore-forming diatoms from the POOZ and PFZ. An increase in the relative abundance of diatom resting spore of *Chaetoceros* subgenus *Hyalochaete* and *Eucampia antarctica* during glacial periods was reported near the continental shelf (Pesjak et al., 2023), close to island systems (Civel-Mazens et al., 2024), but also in the open water of the SO (Abelmann et al., 2006; Jacot Des Combes et al., 2008). A direct quantitative link has already been established between diatom resting spore formation and POC export pulses downstream island plateaus where resting spore formation can account for 40-60 % of the annual POC export (Salter et al., 2012; Rembauville et al., 2015, 2016b). Diatom resting spores were reported to be associated with ice-related species such as *Fragilariopsis curta* and *F. cylindrus* in both modern and glacial sediment cores samples (Leventer, 1991; Armand et al., 2005; Abelmann et al., 2006). Copepod and krill feed on these ice-associated diatoms during late winter and early spring (O'Brien et al., 2011; Schmidt et al., 2014; Pauli et al., 2021) and are efficient vectors of POC export through vertical migration and fecal pellet production (Smith et al., 2025).

https://doi.org/10.5194/egusphere-2025-6347
Preprint. Discussion started: 15 January 2026

Zooplankton-driven export can represent up to 90 % of the annual POC export in productive environments (Manno et al., 2015; Belcher et al., 2019). The PIC:POC ratio is positively correlated with warm water diatom species from the SAZ but negatively correlated with ice-associated diatoms. It has been previously reported that the PIC:POC export ratio increases northward concomitantly with an increase in the abundance of foraminifer and pteropod (Salter et al., 2014; Manno et al., 2022), whereas the PIC:POC export ratio is generally lower southward where the coccolithophores contribution to the calcifying plankton community increases (Rembauville et al., 2016a). Although the calcifying plankton is not explicitly taken into account in this study, diatom communities appears to capture efficiently the ecosystem structure that sets the magnitude of the carbonate counter-pump.

4.2 Local comparisons of the reconstructed fluxes with previously published data

We compare the reconstructed POC flux and PIC:POC export ratio with previously published geochemical data for four sediment cores of the POOZ to estimate the validity of the reconstructed signals and identify potential mechanisms likely to explain the observed glacial/interglacial changes.

In core PS1768-8 (Atlantic sector), periods of high POC fluxes match increases in dust flux and decreases in atmospheric CO_2 (Fig. 8a). The POC flux variations coincides with that of the total organic carbon (TOC) content (Fig. 8b) and shows high values associated with high IRD abundance during MIS 2 and MIS 6 (Fig. 8d). Peaks in PIC:POC ratio and $CaCO_3$ content occur in the absence of IRD during the Holocene and during MIS 5 at 80 ka and 120 ka. The reconstructed PIC:POC export ratio is globally correlated with the $CaCO_3$ content, with higher values during interglacials and lower values during cold periods (Fig 8c).

https://doi.org/10.5194/egusphere-2025-6347
Preprint. Discussion started: 15 January 2026

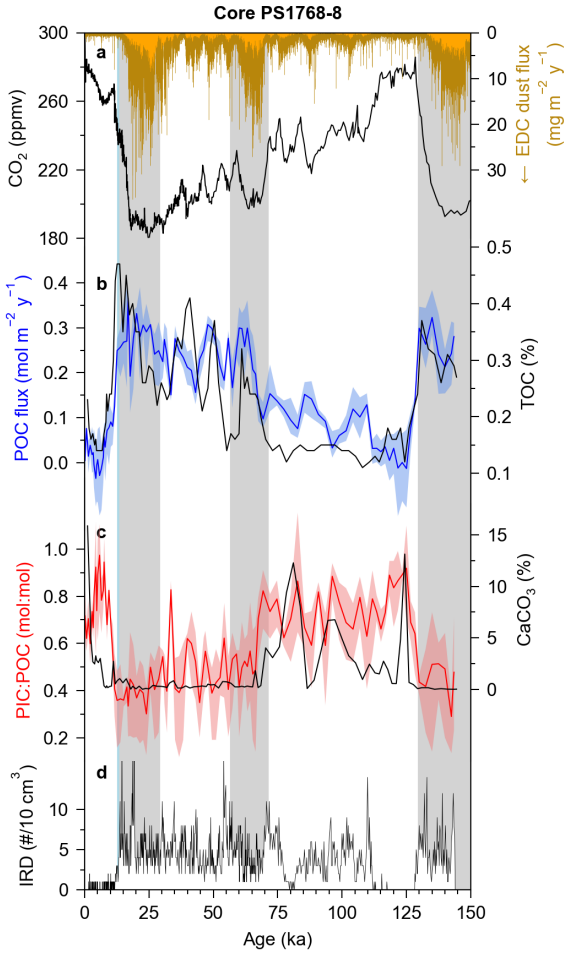

307 **Figure 8.** Comparison of the reconstructed POC export flux and PIC:POC ratio with previously published data for core
308 PS1768-8. a) Atmospheric CO_2 (black, Bereiter et al., 2015) and dust flux (brow, Lambert et al., 2012) from EPICA Dome C
309 (EDC) ice core. b) Reconstructed deep-ocean POC flux (blue, this study) and sediment total organic carbon (TOC) content
310 (black, Kuhn and Bohrmann, 1996). c) Reconstructed PIC:POC export ratio (red, this study) and sediment $CaCO_3$ content
311 (black, Kuhn and Bohrmann, 1996). d) Ice rafted debris (IRD) abundance (Diekmann et al., 1996). In b) and c), the
312 continuous line is the transfer functions average and the colored area is the transfer functions envelope. Grey and blue bars
313 as in Fig. 6.

https://doi.org/10.5194/egusphere-2025-6347
Preprint. Discussion started: 15 January 2026

In core PS1786-1 (Atlantic sector), the highest POC flux of 0.3 mol m^{-2} d^{-1} during the LGM is concomitant high dust flux, low atmospheric CO_2 (Fig. 9a) and high diatom-bound $\delta^{15}N$ values (Fig. 9b). The large POC flux and diatom-bound $\delta^{15}N$ decreases between ca. 18 and 15 ka are concomitant. However, during the late Holocene the two signals are not correlated. Contrary to core PS1768-8, the reconstructed PIC:POC export ratio is not correlated with the $CaCO_3$ content (Fig. 9c), but the latter must be taken with caution as the sediment core depth (5862 m b.s.l.) is deeper that the carbonate compensation depth, suggesting $CaCO_3$ dissolution. Decreases in the PIC:POC ratio are associated with increases in the abundance of IRD during MIS 2, when the higher IRD accumulations occurred.

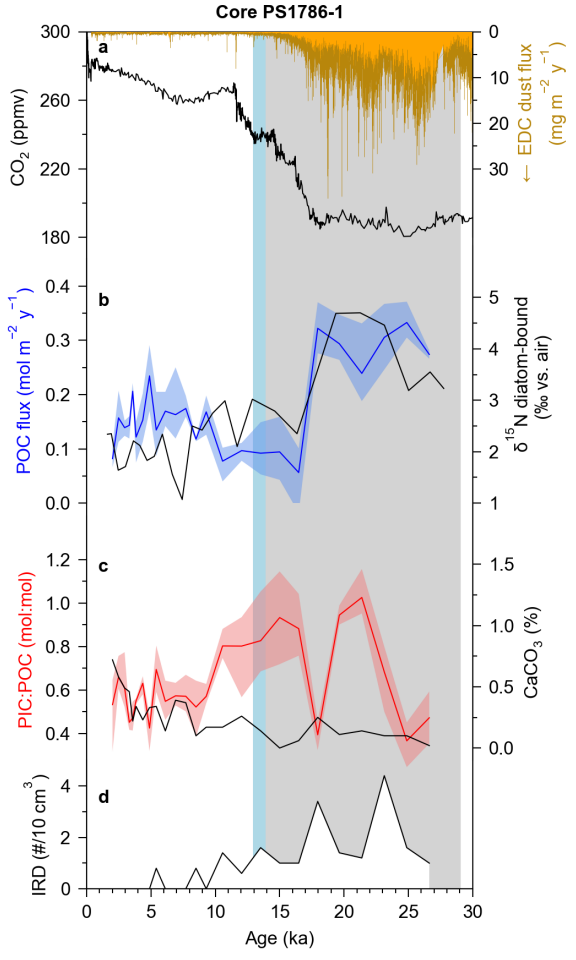

Figure 9. Comparison of the reconstructed POC flux and PIC:POC ratio with previously published data for core PS1786-1. a) Atmospheric CO_2 (black, Bereiter et al., 2015) and dust flux (brown, Lambert et al., 2012) from EPICA Dome C (EDC) ice core. b) Reconstructed deep-ocean POC flux (blue, this study) and diatom-bound $\delta^{15}N$ (black, Jacot Des Combes et al., 2008). c) Reconstructed PIC:POC export ratio (red, this study) and sediment core $CaCO_3$ content (black, Grobe, 1996). d) Ice rafted debris (IRD) abundance (Grobe, 1996). In b) and c), the continuous line is the transfer functions average and the colored area is the transfer functions envelope. Grey and blue bars as in Fig. 6.

https://doi.org/10.5194/egusphere-2025-6347
Preprint. Discussion started: 15 January 2026

In core PS2606-6 (Indian sector), the highest POC flux (0.3-0.4 mol m^{-2} y^{-1}) is again concomitant with high dust and low atmospheric CO_2 during MIS 2 but is not correlated with the low diatom-bound $\delta^{15}N$ values (1-2 ‰) between ca. 25 ka and 18 ka (Fig. 10a, b). However, both records seem to co-evolve around the ACR from ca. 18 ka to 10 ka. The PIC:POC ratio increases from 0.3 to 1 between the LGM and the beginning of the Holocene which is matched by the abrupt increase in the $CaCO_3$ content from 0 to 12 % between 18 ka and 12 ka (Fig. 10c).

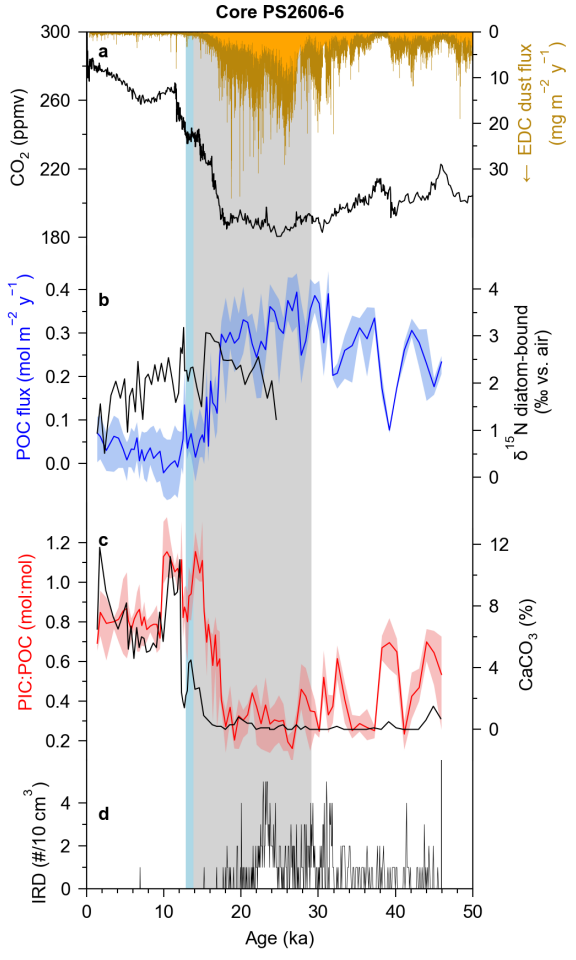

Figure 10. Comparison of the reconstructed POC export flux and PIC:POC ratio with previously published data for core PS2606-6. a) Atmospheric CO_2 (black, Bereiter et al., 2015) and dust flux (brown, Lambert et al., 2012) from EPICA Dome C (EDC) ice core. b) Reconstructed deep-ocean POC flux (this study) and diatom-bound $\delta^{15}N$ (Jacot Des Combes et al., 2008). c) Reconstructed PIC:POC export ratio (this study) and sediment core $CaCO_3$ content (Kuhn, 2003). d) Ice rafted debris (IRD) abundance (Grobe, 2001). In b) and c), the continuous line is the transfer functions average and the colored area is the transfer functions envelope. Grey and blue bars as in Fig. 6.

https://doi.org/10.5194/egusphere-2025-6347
Preprint. Discussion started: 15 January 2026

In core PS75/72-4 (Pacific sector), high POC fluxes are again concomitant with high dust fluxes and high IRD abundance during MIS 2 and MIS 6 (IRD are not quantified in core PS75/072-4, data comes from two cores RS15-LC48 and V1439 located in the southern and northern parts of the Pacific sector, respectively). The MIS 5 shows short events of increased POC flux associated with increased dust fluxes at 80-85 ka and 105-110 ka (Fig. 11a, b). The POC flux closely matches the diatom-bound $\delta^{15}N$ although the correlation is less evident when considering only the centric diatoms (Fig. 11b). The PIC:POC export ratio is higher at the beginning of MIS 5 and decreases during MIS 2-4 and MIS 6 (Fig. 11c). The Ba/Fe ratio is negatively correlated with the reconstructed POC flux and the diatom-bound $\delta^{15}N$ but is positively correlated with the PIC:POC export ratio (Fig. 11c).

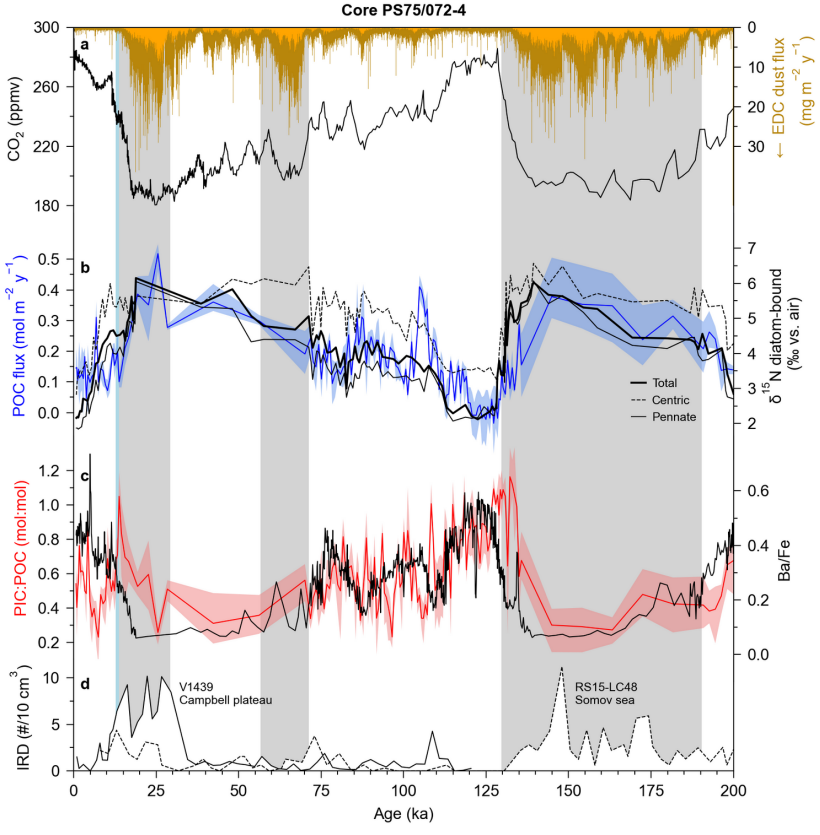

Figure 11. Comparison of the reconstructed POC export flux and PIC:POC ratio with previously published data for core PS75/072-4. a) Atmospheric CO_2 (black, Bereiter et al., 2015) and dust flux (brown, Lambert et al., 2012) from EPICA Dome C (EDC) ice core. b) Reconstructed deep-ocean POC flux (blue, this study) and diatom-bound $\delta^{15}N$ (black, Studer et al., 2015). c) Reconstructed PIC:POC export ratio (red, this study) and sediment Ba/Fe elemental ratio (black, Studer et al., 2015). d) Ice rafted debris (IRD) abundance from other cores in the Pacific sector : the Somov sea (McKay et al., 2022) and the Campbell plateau (Carter et al., 2002). In b) and c), the continuous line is the transfer functions average and the colored area is the transfer functions envelope. Grey and blue bars as in Fig. 6.

https://doi.org/10.5194/egusphere-2025-6347
Preprint. Discussion started: 15 January 2026

4.3 Consistency of the reconstructed biological and carbonate pump during glacial/interglacial periods

At the global SO scale, we report a two times higher deep-ocean POC flux during MIS 2 compared to the Holocene and a 1.5 times higher flux compared to the modern sediment trap average. This is consistent with modeling studies that quantified the difference in the upper-ocean (~100 m) POC export between the LGM and the preindustrial era in the SO : +20 % (Bopp et al., 2003), +20 % to +80 % (Tagliabue et al., 2009), +0 % to +300 % (Lambert et al., 2015), +40 % (Yamamoto et al., 2019). There are fewer estimates of the PIC:POC ratio during the LGM. At global scale, the modeling study by Bopp et al. (2003) suggested a LGM PIC:POC export ratio 8 % lower than preindustrial, in agreement with our SO estimate of 13 % and 17 % lower MIS2 value compared to modern sediment trap data and Holocene, respectively.

Several studies previously proposed that during glacial or colder periods, export production increased in the SAZ due to iron fertilization while it decreased in the AZ due to lower nitrate utilization associated with higher ocean vertical stratification (François et al., 1997; Jaccard et al., 2013; Gottschalk et al., 2016; Sigman et al., 2021). In these studies, export estimates in the SAZ are based on alkenone flux and/or $\delta^{15}N$, while in the AZ they are based on the Ba/Fe ratio, opal flux or $\delta^{15}N$ proxies. Contrasting with these findings, our study shows that the reconstructed POC export flux increases during glacial periods in the AZ, associated with high IRD inputs and high atmospheric dust flux. In core PS75/072-4, during MIS 5, the reconstructed POC flux decreases while the Ba/Fe ratio increases together with the reconstructed PIC:POC ratio (Fig. 11c). The Ba/Fe carbon export proxy is associated with several potential limitations when applied to SO sediment cores such as variations in dissolved Ba in oceanic waters and variations in barite preservation in organic matter-rich sediments (François et al., 1997; Averyt and Paytan, 2004; Hernandez-Sanchez et al., 2011). Higher PIC export and lower organic carbon accumulation during warm periods might cause a lower sedimentary TOC content leading to a better preservation of barite in sediments, hence increasing the Ba/Fe ratio. The sensitivity of the Ba/Fe proxy to organic matter content might thus explain the discrepancy between our reconstructed POC flux and the Ba/Fe elemental ratio.

The reconstructed POC flux increase is highly correlated with diatom-bound $\delta^{15}N$ in core PS75/072-4 (Fig. 8b) and with TOC in core PS1768-8 (Fig. 11b). Diatom-bound $\delta^{15}N$ reflects the degree of nitrate utilization by phytoplankton (Altabet and Francois, 1994). During glacial periods in the AZ, high diatom-bound $\delta^{15}N$ associated with low opal accumulation rate have been interpreted as a more complete nitrate utilization caused by lower nitrate supply in the surface ocean due to higher vertical stratification, ultimately resulting in lower opal export fluxes (Studer et al., 2015). Our new transfer functions show an increase in deep-ocean POC export in the AZ during glacial periods, which could appear as inconsistent with lower opal export flux. However, if there is a shift from a high to low biogenic silica to POC ratio diatom community, a decrease in flux opal flux can occur (Assmy et al., 2013; Tréguer et al., 2018). Hence, the reconstructed glacial increase of POC flux associated with a decrease in opal flux is coherent with a diatom community shift from silica to carbon sinkers together with a higher zooplankton contribution to the total POC export flux.

https://doi.org/10.5194/egusphere-2025-6347
Preprint. Discussion started: 15 January 2026

4.4 Processes driving the biological pump and carbonate counter-pump changes in the Antarctic Zone

The global biological pump efficiency can be decomposed into two critical steps quantified by export efficiency and transfer efficiency. Export efficiency refers to the proportion of the primary production that is exported out of the mixed layer, and transfer efficiency is the fraction of exported organic matter that is not remineralized in the mesopelagic zone and reaches the deep ocean >1000 m (Henson et al., 2012; Doney et al., 2024). The analysis of the detrital fraction in sediment cores suggests that both the SAZ and the AZ were fertilized by atmospheric dust deposition during glacial periods (Struve et al., 2020). Iron fertilization could lead to the higher macronutrient utilization in the AZ deduced from increased diatom-bound $\delta^{15}N$, hence resulting in higher export efficiency mediated by bloom-forming and spore-forming diatoms (Blain et al., 2021), in agreement with the original iron hypothesis (Martin, 1990; Moore et al., 2000). Moreover, we observe a tight coupling between markers of ice presence (IRD) and increases in the reconstructed deep-ocean POC flux. The northward migration of the winter sea-ice edge during glacial periods (Crosta et al., 2022) could contribute to the increase in the large zooplankton-mediated POC export, increasing transfer efficiency. Hence, both the dust fertilization and the extended sea ice area could drive a globally more efficient biological pump during glacial periods.

The Atlantic record of core PS1768-8 shows an elevated POC flux throughout MIS 2 (Fig. 8b) whereas in the Indian and Pacific sector the POC export starts to decrease earlier, around 20 ka (Fig. 10b, 11b). This might result from two processes : different iron fertilization and/or different timing of deglaciation. Model results suggest that LGM dust fluxes where higher in the Atlantic sector, potentially leading to higher export production when compared to the other SO sectors (Lambert et al., 2015). In the Atlantic core PS1768-8, the high IRD abundance until the end of MIS 2 (Fig. 8d) suggests a longer influence of sea ice extension compared to core PS2606 in the Indian sector (Fig. 10d). Crosta et al. (2022) suggested an earlier ice retreat in the Pacific when compared to the two other sectors, although the timing of the ice retreat is not well constrained in all the SO sectors. Reconstructions for the high temporal resolution cores PS97/72-1 and COR1GC shows that there is a substantial increase in POC export during the ACR (Fig. 6a, d). As sea ice extension notably increased during ACR (Vorrath et al., 2023), our results suggest a coupling at short time scale between changes in sea ice extension and deep-ocean POC export, supporting the idea of sea ice as an important factor driving plankton community composition and the efficiency of the biological pump (Moore et al., 2000).

The increase in the reconstructed PIC:POC ratio during deglaciations in the three sectors of the SO is tightly coupled with the decrease in IRD in SO sediments. This observation is consistent with enhanced coccolith export related to the rising sea surface temperatures and decreasing sea ice extension (Duchamp-Alphonse et al., 2018). While there is a similar higher MIS 2 POC flux in the three sector of the SO compared to the Holocene (Fig. 7a), the reconstructed MIS 2 PIC:POC export ratio in the Pacific is higher than that of the two other sectors (Fig. 7b). This geographical contrast suggests a sector-specific response of the calcifying plankton community during glacial conditions. Indeed, studies have demonstrated that coccolithophores dominates the PIC in the PFZ of the Pacific Ocean, where they are mostly represented by *Emiliania huxleyi* morphogroup B that is rare in other high latitude environments (Saavedra-Pellitero et al., 2014, 2025). Coccolithophores biogeography might be responsible for the specifically high MIS 2 PIC:POC export ratio of the Pacific sector compared to the Atlantic and the Indian sectors, although a direct quantification and identification of coccoliths the sediment cores are necessary to confirm this hypothesis.

https://doi.org/10.5194/egusphere-2025-6347
Preprint. Discussion started: 15 January 2026

5 Conclusion

The compilation of sediment trap and sediment core datasets from the SO allowed us to create three new independent transfer functions to reconstruct deep-ocean POC export flux and PIC:POC ratio. The three methods (MLR, PLSR, GBR) used to design these transfer functions provide convergent results, however the PLSR and GBR approaches are associated with lower errors. The factor analysis associated with the MLR allows to identify ecologically-consistent diatom groups associated with POC export and PIC:POC ratio. High POC export is correlated with bloom-forming and resting spores-forming diatoms, as well as sea ice-related diatoms. High PIC:POC ratio is associated with warmer SAZ diatom species. Indeed, the number of sediment trap data is an inherent limitation to the precision of the transfer functions. Hence, to improve these, the sediment trap sampling effort conducted during the 1990-2010 period must be continued. Furthermore, standard deployment depth and sampling frequency coupled with a homogeneous diatom identification procedure would also increase transfer functions quality.

Based on nine sediment cores located in the three sectors of the SO, we show a POC export increase during glacial periods in the AZ. This result is in agreement with studies based on diatom-bound $\delta^{15}N$ and total organic carbon content but contradicts results based on the Ba/Fe ratio proxy. We argue that preservation of Ba in SO sediments could potentially hinder the use of this latter proxy. To explain the glacial increase of POC flux observed in the AZ of the global SO, we suggest that dust-induced iron fertilization together with a northward migration of the sea ice edge during glacial periods lead to a stronger biological pump resulting from the direct export of bloom-forming diatom combined with higher export of zooplankton feeding on ice-associated diatoms. This concept is consistent with the first estimate of glacial SO CO_2 sink (Moore et al., 2000) and with more recent estimates of nutrient utilization in the SAZ and AZ (Wang et al., 2017). We also show that the PIC:POC ratio increases during deglaciation, in agreement with the previously proposed view of a stronger carbonate counter-pump caused by the concomitant development of calcifying plankton in warmer water. Our results highlight the role of SO biology in lowering atmospheric CO_2 during the LGM as the result of a higher biological pump (+50 %) and a lower carbonate counter-pump (-17 %) compared to the Holocene. The application of the new proxies presented in this study to sediment cores of from the SAZ could allow a direct comparison of the two SO zones, leading to a better comprehension of the latitudinal response of the biological pump and carbonate counter-pump during glacial periods and at the glacial-interglacial transitions.

Code and data availability

The python scripts and the sediment trap and sediment core datasets will be made available on public repositories in case of acceptation of the present manuscript.

Authors contribution

MR performed the conceptualization, data curation, formal analysis, and wrote the original manuscript. S. P. reviewed and edited the manuscript.

https://doi.org/10.5194/egusphere-2025-6347
Preprint. Discussion started: 15 January 2026

Competing interests

The contact author has declared that none of the authors has any competing interests.

Financial support

This study was supported by CNRS INSU LEFE 'DUST' funding to S. Pichat and ANR EXODUST (ANR-24-CE01-6090).

References

Abelmann, A. and Gersonde, R.: Biosiliceous particle flux in the Southern Ocean, Mar. Chem., 35, 503–536, https://doi.org/10.1016/S0304-4203(09)90040-8, 1991.

Abelmann, A., Gersonde, R., Cortese, G., Kuhn, G., and Smetacek, V.: Extensive phytoplankton blooms in the Atlantic sector of the glacial Southern Ocean, Paleoceanography, 21, https://doi.org/10.1029/2005PA001199, 2006.

Altabet, M. A. and Francois, R.: Sedimentary nitrogen isotopic ratio as a recorder for surface ocean nitrate utilization, Glob. Biogeochem. Cycles, 8, 103–116, https://doi.org/10.1029/93GB03396, 1994.

Anderson, H. J., Chase, Z., Bostock, H. C., Noble, T. L., Shuttleworth, R., Taiapa, B., Chen, W. H., Ren, H., and Jacobsen, G. E.: Millennial-Scale Carbon Flux Variability in the Subantarctic Pacific During Marine Isotope Stage 3 (57–29 ka), Paleoceanogr. Paleoclimatology, 39, e2023PA004776, https://doi.org/10.1029/2023PA004776, 2024.

Archer, D., Winguth, A., Lea, D., and Mahowald, N.: What caused the glacial/interglacial atmospheric pCO2 cycles?, Rev. Geophys., 38, 159–189, https://doi.org/10.1029/1999RG000066, 2000.

Armand, L. K., Crosta, X., Romero, O., and Pichon, J.-J.: The biogeography of major diatom taxa in Southern Ocean sediments: 1. Sea ice related species, Palaeogeogr. Palaeoclimatol. Palaeoecol., 223, 93–126, https://doi.org/10.1016/j.palaeo.2005.02.015, 2005.

Assmy, P., Smetacek, V., Montresor, M., Klaas, C., Henjes, J., Strass, V. H., Arrieta, J. M., Bathmann, U., Berg, G. M., Breitbarth, E., Cisewski, B., Friedrichs, L., Fuchs, N., Herndl, G. J., Jansen, S., Krägefsky, S., Latasa, M., Peeken, I., Röttgers, R., Scharek, R., Schüller, S. E., Steigenberger, S., Webb, A., and Wolf-Gladrow, D.: Thick-shelled, grazer-protected diatoms decouple ocean carbon and silicon cycles in the iron-limited Antarctic Circumpolar Current, Proc. Natl. Acad. Sci. U. S. A., 110, 20633–20638, https://doi.org/10.1073/pnas.1309345110, 2013.

Averyt, K. B. and Paytan, A.: A comparison of multiple proxies for export production in the equatorial Pacific, Paleoceanography, 19, https://doi.org/10.1029/2004PA001005, 2004.

de Baar, H. J. W., Buma, A. G. J., Nolting, R. F., Cadée, G. C., Jacques, G., and Tréguer, P. J.: On iron limitation of the Southern Ocean: experimental observations in the Weddell and Scotia Seas, Mar. Ecol. Prog. Ser., 65, 105–122, 1990.

Belcher, A., Henson, S. A., Manno, C., Hill, S. L., Atkinson, A., Thorpe, S. E., Fretwell, P., Ireland, L., and Tarling, G. A.: Krill faecal pellets drive hidden pulses of particulate organic carbon in the marginal ice zone, Nat. Commun., 10, 889, https://doi.org/10.1038/s41467-019-08847-1, 2019.

Benz, V., Esper, O., Gersonde, R., Lamy, F., and Tiedemann, R.: Last Glacial Maximum sea surface temperature and sea-ice extent in the Pacific sector of the Southern Ocean, Quat. Sci. Rev., 146, 216–237, https://doi.org/10.1016/j.quascirev.2016.06.006, 2016.

https://doi.org/10.5194/egusphere-2025-6347
Preprint. Discussion started: 15 January 2026

Bereiter, B., Eggleston, S., Schmitt, J., Nehrbass-Ahles, C., Stocker, T. F., Fischer, H., Kipfstuhl, S., and Chappellaz, J.: Revision of the EPICA Dome C CO2 record from 800 to 600 kyr before present, Geophys. Res. Lett., 42, 542–549, https://doi.org/10.1002/2014GL061957, 2015.

Berner, K. S., Koç, N., Divine, D., Godtliebsen, F., and Moros, M.: A decadal-scale Holocene sea surface temperature record from the subpolar North Atlantic constructed using diatoms and statistics and its relation to other climate parameters, Paleoceanography, 23, https://doi.org/10.1029/2006PA001339, 2008.

Blain, S., Rembauville, M., Crispi, O., and Obernosterer, I.: Synchronized autonomous sampling reveals coupled pulses of biomass and export of morphologically different diatoms in the Southern Ocean, Limnol. Oceanogr., 66, 753–764, https://doi.org/10.1002/lno.11638, 2021.

Blain, S., Planquette, H., Obernosterer, I., and Guéneuguès, A.: Vertical Flux of Trace Elements Associated With Lithogenic and Biogenic Carrier Phases in the Southern Ocean, Glob. Biogeochem. Cycles, 36, e2022GB007371, https://doi.org/10.1029/2022GB007371, 2022.

Bopp, L., Kohfeld, K. E., Le Quéré, C., and Aumont, O.: Dust impact on marine biota and atmospheric CO2 during glacial periods, Paleoceanography, 18, https://doi.org/10.1029/2002PA000810, 2003.

Brandon, M., Duchamp-Alphonse, S., Michel, E., Landais, A., Isguder, G., Richard, P., Pige, N., Bassinot, F., Jaccard, S. L., and Bartolini, A.: Enhanced Carbonate Counter Pump and upwelling strengths in the Indian sector of the Southern Ocean during MIS 11, Quat. Sci. Rev., 287, 107556, https://doi.org/10.1016/j.quascirev.2022.107556, 2022.

Carter, L., Neil, H. L., and Northcote, L.: Late Quaternary ice-rafting events in the SW Pacific Ocean, off eastern New Zealand, Mar. Geol., 191, 19–35, https://doi.org/10.1016/S0025-3227(02)00509-1, 2002.

Cattell, R. B.: The Scree Test For The Number Of Factors, Multivar. Behav. Res., 1, 245–276, https://doi.org/10.1207/s15327906mbr0102_10, 1966.

Civel-Mazens, M., Crosta, X., Cortese, G., Lowe, V., Itaki, T., Ikehara, M., and Kohfeld, K.: Subantarctic jet migrations regulate vertical mixing in the Southern Indian, Earth Planet. Sci. Lett., 642, 118877, https://doi.org/10.1016/j.epsl.2024.118877, 2024.

Crosta, X., Pichon, J.-J., and Burckle, L. H.: Application of modern analog technique to marine Antarctic diatoms: Reconstruction of maximum sea-ice extent at the Last Glacial Maximum, Paleoceanography, 13, 284–297, https://doi.org/10.1029/98PA00339, 1998.

Crosta, X., Kohfeld, K. E., Bostock, H. C., Chadwick, M., Du Vivier, A., Esper, O., Etourneau, J., Jones, J., Leventer, A., Müller, J., Rhodes, R. H., Allen, C. S., Ghadi, P., Lamping, N., Lange, C. B., Lawler, K.-A., Lund, D., Marzocchi, A., Meissner, K. J., Menviel, L., Nair, A., Patterson, M., Pike, J., Prebble, J. G., Riesselman, C., Sadatzki, H., Sime, L. C., Shukla, S. K., Thöle, L., Vorrath, M.-E., Xiao, W., and Yang, J.: Antarctic sea ice over the past 130 000 years – Part 1: a review of what proxy records tell us, Clim. Past, 18, 1729–1756, https://doi.org/10.5194/cp-18-1729-2022, 2022.

Diekmann, B., Fütterer, D. K., Grobe, H., Hillenbrand, C.-D., Kuhn, G., Michels, K., Petschick, R., and Pirrung, M.: Ice rafted debris (> 2 mm gravel) distribution in sediment core PS1768-8, https://doi.org/10.1594/PANGAEA.50243, 1996.

Doney, S. C., Mitchell, K. A., Henson, S. A., Cavan, E., DeVries, T., Gruber, N., Hauck, J., Mouw, C. B., Müller, J. D., and Primeau, F. W.: Observational and Numerical Modeling Constraints on the Global Ocean Biological Carbon Pump, Glob. Biogeochem. Cycles, 38, e2024GB008156, https://doi.org/10.1029/2024GB008156, 2024.

Duchamp-Alphonse, S., Siani, G., Michel, E., Beaufort, L., Gally, Y., and Jaccard, S. L.: Enhanced ocean-atmosphere carbon partitioning via the carbonate counter pump during the last deglacial, Nat. Commun., 9, 2396, https://doi.org/10.1038/s41467-018-04625-7, 2018.

https://doi.org/10.5194/egusphere-2025-6347
Preprint. Discussion started: 15 January 2026

Dymond, J., Suess, E., and Lyle, M.: Barium in Deep-Sea Sediment: A Geochemical Proxy for Paleoproductivity, Paleoceanography, 7, 163–181, https://doi.org/10.1029/92PA00181, 1992.

Esper, O. and Gersonde, R.: Quaternary surface water temperature estimations: New diatom transfer functions for the Southern Ocean, Palaeogeogr. Palaeoclimatol. Palaeoecol., 414, 1–19, https://doi.org/10.1016/j.palaeo.2014.08.008, 2014.

Feely, R. A., Sabine, C. L., Lee, K., Berelson, W., Kleypas, J., Fabry, V. J., and Millero, F. J.: Impact of Anthropogenic CO2 on the CaCO3 System in the Oceans, Science, 305, 362–366, https://doi.org/10.1126/science.1097329, 2004.

Fischer, G., Gersonde, R., and Wefer, G.: Organic carbon, biogenic silica and diatom fluxes in the marginal winter sea-ice zone and in the Polar Front Region: interannual variations and differences in composition, Deep Sea Res. Part II Top. Stud. Oceanogr., 49, 1721–1745, https://doi.org/10.1016/S0967-0645(02)00009-7, 2002.

François, R., Altabet, M. A., Yu, E.-F., Sigman, D. M., Bacon, M. P., Frank, M., Bohrmann, G., Bareille, G., and Labeyrie, L. D.: Contribution of Southern Ocean surface-water stratification to low atmospheric CO2 concentrations during the last glacial period, Nature, 389, 929–935, https://doi.org/10.1038/40073, 1997.

Francois, R., Frank, M., Rutgers van der Loeff, M. M., and Bacon, M. P.: 230Th normalization: An essential tool for interpreting sedimentary fluxes during the late Quaternary, Paleoceanography, 19, https://doi.org/10.1029/2003PA000939, 2004.

Frankignoulle, M., Canon, C., and Gattuso, J.-P.: Marine calcification as a source of carbon dioxide: Positive feedback of increasing atmospheric CO2, Limnol. Oceanogr., 39, 458–462, https://doi.org/10.4319/lo.1994.39.2.0458, 1994.

Friedman, J. H.: Greedy function approximation: A gradient boosting machine., Ann. Stat., 29, 1189–1232, https://doi.org/10.1214/aos/1013203451, 2001.

Gersonde, R., Crosta, X., Abelmann, A., and Armand, L.: Sea-surface temperature and sea ice distribution of the Southern Ocean at the EPILOG Last Glacial Maximum—a circum-Antarctic view based on siliceous microfossil records, Quat. Sci. Rev., 24, 869–896, https://doi.org/10.1016/j.quascirev.2004.07.015, 2005.

Gottschalk, J., Skinner, L. C., Lippold, J., Vogel, H., Frank, N., Jaccard, S. L., and Waelbroeck, C.: Biological and physical controls in the Southern Ocean on past millennial-scale atmospheric CO2 changes, Nat. Commun., 7, 11539, https://doi.org/10.1038/ncomms11539, 2016.

Grigorov, I., Rigual-Hernandez, A. S., Honjo, S., Kemp, A. E. S., and Armand, L. K.: Settling fluxes of diatoms to the interior of the Antarctic circumpolar current along 170 °W, Deep Sea Res. Part Oceanogr. Res. Pap., 93, 1–13, https://doi.org/10.1016/j.dsr.2014.07.008, 2014.

Grobe, H.: Sedimentology of core PS1786-1, https://doi.org/10.1594/PANGAEA.51719, 1996.

Grobe, H.: Ice rafted debris (> 2 mm gravel) distribution in sediment core PS2606-6, https://doi.org/10.1594/PANGAEA.58545, 2001.

Henson, S. A., Sanders, R., and Madsen, E.: Global patterns in efficiency of particulate organic carbon export and transfer to the deep ocean, Glob. Biogeochem. Cycles, 26, https://doi.org/10.1029/2011GB004099, 2012.

Henson, S. A., Briggs, N., Carvalho, F., Manno, C., Mignot, A., and Thomalla, S.: A seasonal transition in biological carbon pump efficiency in the northern Scotia Sea, Southern Ocean, Deep Sea Res. Part II Top. Stud. Oceanogr., 208, 105274, https://doi.org/10.1016/j.dsr2.2023.105274, 2023.

Hernandez-Sanchez, M. T., Mills, R. A., Planquette, H., Pancost, R. D., Hepburn, L., Salter, I., and FitzGeorge-Balfour, T.: Quantifying export production in the Southern Ocean: Implications for the Baxs proxy, Paleoceanography, 26, https://doi.org/10.1029/2010PA002111, 2011.

https://doi.org/10.5194/egusphere-2025-6347
Preprint. Discussion started: 15 January 2026

Honjo, S., Francois, R., Manganini, S., Dymond, J., and Collier, R.: Particle fluxes to the interior of the Southern Ocean in the Western Pacific sector along 170°W, Deep Sea Res. Part II Top. Stud. Oceanogr., 47, 3521–3548, https://doi.org/10.1016/S0967-0645(00)00077-1, 2000.

Hutson, W. H.: The Agulhas Current During the Late Pleistocene: Analysis of Modern Faunal Analogs, Science, 207, 64–66, https://doi.org/10.1126/science.207.4426.64, 1980.

Imbrie, J. and Kipp, N. G.: A new micropaleontological method for quantitative paleoclimatology : application to a late Pleistocene Caribbean core, Late Cenozoic Glacial Ages, 71–181, 1971.

Jaccard, S. L., Hayes, C. T., Martínez-García, A., Hodell, D. A., Anderson, R. F., Sigman, D. M., and Haug, G. H.: Two Modes of Change in Southern Ocean Productivity Over the Past Million Years, Science, 339, 1419–1423, https://doi.org/10.1126/science.1227545, 2013.

Jackson, D. A.: Stopping Rules in Principal Components Analysis: A Comparison of Heuristical and Statistical Approaches, Ecology, 74, 2204–2214, https://doi.org/10.2307/1939574, 1993.

Jacot Des Combes, H., Esper, O., De La Rocha, C. L., Abelmann, A., Gersonde, R., Yam, R., and Shemesh, A.: Diatom δ13C, δ15N, and C/N since the Last Glacial Maximum in the Southern Ocean: Potential impact of Species Composition, Paleoceanography, 23, https://doi.org/10.1029/2008PA001589, 2008.

Juggins, S.: Quantitative reconstructions in palaeolimnology: new paradigm or sick science?, Quat. Sci. Rev., 64, 20–32, https://doi.org/10.1016/j.quascirev.2012.12.014, 2013.

Kohfeld, K. E., Quéré, C. L., Harrison, S. P., and Anderson, R. F.: Role of Marine Biology in Glacial-Interglacial CO2 Cycles, Science, 308, 74–78, https://doi.org/10.1126/science.1105375, 2005.

Kuhn, G.: Calcium carbonate content of sediment core PS2606-6, https://doi.org/10.1594/PANGAEA.93723, 2003.

Kuhn, G. and Bohrmann, G.: Sedimentology of core PS1768-8, https://doi.org/10.1594/PANGAEA.51126, 1996.

Lambert, F., Bigler, M., Steffensen, J. P., Hutterli, M., and Fischer, H.: Centennial mineral dust variability in high-resolution ice core data from Dome C, Antarctica, Clim. Past, 8, 609–623, https://doi.org/10.5194/cp-8-609-2012, 2012.

Lambert, F., Tagliabue, A., Shaffer, G., Lamy, F., Winckler, G., Farias, L., Gallardo, L., and De Pol-Holz, R.: Dust fluxes and iron fertilization in Holocene and Last Glacial Maximum climates, Geophys. Res. Lett., 42, 6014–6023, https://doi.org/10.1002/2015GL064250, 2015.

Leventer, A.: Sediment trap diatom assemblages from the northern Antarctic Peninsula region, Deep Sea Res. Part Oceanogr. Res. Pap., 38, 1127–1143, https://doi.org/10.1016/0198-0149(91)90099-2, 1991.

Maloney, K. O., Schmid, M., and Weller, D. E.: Applying additive modelling and gradient boosting to assess the effects of watershed and reach characteristics on riverine assemblages, Methods Ecol. Evol., 3, 116–128, https://doi.org/10.1111/j.2041-210X.2011.00124.x, 2012.

Manno, C., Stowasser, G., Enderlein, P., Fielding, S., and Tarling, G. A.: The contribution of zooplankton faecal pellets to deep-carbon transport in the Scotia Sea (Southern Ocean), Biogeosciences, 12, 1955–1965, https://doi.org/10.5194/bg-12-1955-2015, 2015.

Manno, C., Stowasser, G., Fielding, S., Apeland, B., and Tarling, G. A.: Deep carbon export peaks are driven by different biological pathways during the extended Scotia Sea (Southern Ocean) bloom, Deep Sea Res. Part II Top. Stud. Oceanogr., 205, 105183, https://doi.org/10.1016/j.dsr2.2022.105183, 2022.

https://doi.org/10.5194/egusphere-2025-6347
Preprint. Discussion started: 15 January 2026

Marsay, C. M., Sanders, R. J., Henson, S. A., Pabortsava, K., Achterberg, E. P., and Lampitt, R. S.: Attenuation of sinking particulate organic carbon flux through the mesopelagic ocean, Proc. Natl. Acad. Sci., 112, 1089–1094, https://doi.org/10.1073/pnas.1415311112, 2015.

Martin, J. H.: Glacial-interglacial CO2 change: The Iron Hypothesis, Paleoceanography, 5, 1–13, https://doi.org/10.1029/PA005i001p00001, 1990.

Martin, J. H., Knauer, G. A., Karl, D. M., and Broenkow, W. W.: VERTEX: carbon cycling in the northeast Pacific, Deep Sea Res. Part Oceanogr. Res. Pap., 34, 267–285, https://doi.org/10.1016/0198-0149(87)90086-0, 1987.

Martínez-García, A., Sigman, D. M., Ren, H., Anderson, R. F., Straub, M., Hodell, D. A., Jaccard, S. L., Eglinton, T. I., and Haug, G. H.: Iron Fertilization of the Subantarctic Ocean During the Last Ice Age, Science, 343, 1347–1350, https://doi.org/10.1126/science.1246848, 2014.

McKay, R., Albot, O., Dunbar, G. B., Lee, J. I., Lee, M. K., Yoo, K.-C., Kim, S., Turton, N., Kulhanek, D., Patterson, M., and Levy, R.: A Comparison of Methods for Identifying and Quantifying Ice Rafted Debris on the Antarctic Margin, Paleoceanogr. Paleoclimatology, 37, e2021PA004404, https://doi.org/10.1029/2021PA004404, 2022.

Moore, J. K., Abbott, M. R., Richman, J. G., and Nelson, D. M.: The southern ocean at the Last Glacial Maximum: A strong sink for atmospheric carbon dioxide, Glob. Biogeochem. Cycles, 14, 455–475, https://doi.org/10.1029/1999GB900051, 2000.

O'Brien, C., Virtue, P., Kawaguchi, S., and Nichols, P. D.: Aspects of krill growth and condition during late winter-early spring off East Antarctica (110–130°E), Deep Sea Res. Part II Top. Stud. Oceanogr., 58, 1211–1221, https://doi.org/10.1016/j.dsr2.2010.11.001, 2011.

Orme, L. C., Crosta, X., Miettinen, A., Divine, D. V., Husum, K., Isaksson, E., Wacker, L., Mohan, R., Ther, O., and Ikehara, M.: Sea surface temperature in the Indian sector of the Southern Ocean over the Late Glacial and Holocene, Clim. Past, 16, 1451–1467, https://doi.org/10.5194/cp-16-1451-2020, 2020.

Pauli, N.-C., Metfies, K., Pakhomov, E. A., Neuhaus, S., Graeve, M., Wenta, P., Flintrop, C. M., Badewien, T. H., Iversen, M. H., and Meyer, B.: Selective feeding in Southern Ocean key grazers—diet composition of krill and salps, Commun. Biol., 4, 1061, https://doi.org/10.1038/s42003-021-02581-5, 2021.

Pedregosa, F., Varoquaux, G., Gramfort, A., Michel, V., Thirion, B., Grisel, O., Blondel, M., Prettenhofer, P., Weiss, R., Dubourg, V., Vanderplas, J., Passos, A., Cournapeau, D., Brucher, M., Perrot, M., and Duchesnay, É.: Scikit-learn: Machine Learning in Python, J. Mach. Learn. Res., 12, 2825–2830, 2011.

Pesjak, L., McMinn, A., Chase, Z., and Bostock, H.: Sea ice and productivity changes over the last glacial cycle in the Adélie Land region, East Antarctica, based on diatom assemblage variability, Clim. Past, 19, 419–437, https://doi.org/10.5194/cp-19-419-2023, 2023.

Petit, J. R., Jouzel, J., Raynaud, D., Barkov, N. I., Barnola, J.-M., Basile, I., Bender, M., Chappellaz, J., Davis, M., Delaygue, G., Delmotte, M., Kotlyakov, V. M., Legrand, M., Lipenkov, V. Y., Lorius, C., PÉpin, L., Ritz, C., Saltzman, E., and Stievenard, M.: Climate and atmospheric history of the past 420,000 years from the Vostok ice core, Antarctica, Nature, 399, 429–436, https://doi.org/10.1038/20859, 1999.

Pudsey, C. J. and King, P.: Particle fluxes, benthic processes and the palaeoenvironmental record in the Northern Weddell Sea, Deep Sea Res. Part Oceanogr. Res. Pap., 44, 1841–1876, https://doi.org/10.1016/S0967-0637(97)00064-2, 1997.

Ran, L., Wiesner, M. G., Liang, Y., Liang, W., Zhang, L., Yang, Z., Li, H., and Chen, J.: Differential dissolution of biogenic silica significantly affects the utility of sediment diatoms as paleoceanographic proxies, Limnol. Oceanogr., 69, 467–481, https://doi.org/10.1002/lno.12492, 2024.

https://doi.org/10.5194/egusphere-2025-6347
Preprint. Discussion started: 15 January 2026

Rembauville, M., Blain, S., Armand, L., Quéguiner, B., and Salter, I.: Export fluxes in a naturally iron-fertilized area of the Southern Ocean – Part 2: Importance of diatom resting spores and faecal pellets for export, Biogeosciences, 12, 3171–3195, https://doi.org/10.5194/bg-12-3171-2015, 2015.

Rembauville, M., Meilland, J., Ziveri, P., Schiebel, R., Blain, S., and Salter, I.: Planktic foraminifer and coccolith contribution to carbonate export fluxes over the central Kerguelen Plateau, Deep Sea Res. Part Oceanogr. Res. Pap., 111, 91–101, https://doi.org/10.1016/j.dsr.2016.02.017, 2016a.

Rembauville, M., Manno, C., Tarling, G. A., Blain, S., and Salter, I.: Strong contribution of diatom resting spores to deep-sea carbon transfer in naturally iron-fertilized waters downstream of South Georgia, Deep Sea Res. Part Oceanogr. Res. Pap., 115, 22–35, https://doi.org/10.1016/j.dsr.2016.05.002, 2016b.

Rembauville, M., Briggs, N., Ardyna, M., Uitz, J., Catala, P., Penkerc'h, C., Poteau, A., Claustre, H., and Blain, S.: Plankton Assemblage Estimated with BGC-Argo Floats in the Southern Ocean: Implications for Seasonal Successions and Particle Export, J. Geophys. Res. Oceans, 122, 8278–8292, https://doi.org/10.1002/2017JC013067, 2017.

Rigual-Hernández, A. S., Trull, T. W., Bray, S. G., Cortina, A., and Armand, L. K.: Latitudinal and temporal distributions of diatom populations in the pelagic waters of the Subantarctic and Polar Frontal zones of the Southern Ocean and their role in the biological pump, Biogeosciences, 12, 5309–5337, https://doi.org/10.5194/bg-12-5309-2015, 2015a.

Rigual-Hernández, A. S., Trull, T. W., Bray, S. G., Closset, I., and Armand, L. K.: Seasonal dynamics in diatom and particulate export fluxes to the deep sea in the Australian sector of the southern Antarctic Zone, J. Mar. Syst., 142, 62–74, https://doi.org/10.1016/j.jmarsys.2014.10.002, 2015b.

Rigual-Hernández, A. S., Pilskaln, C. H., Cortina, A., Abrantes, F., and Armand, L. K.: Diatom species fluxes in the seasonally ice-covered Antarctic Zone: New data from offshore Prydz Bay and comparison with other regions from the eastern Antarctic and western Pacific sectors of the Southern Ocean, Deep Sea Res. Part II Top. Stud. Oceanogr., 161, 92–104, https://doi.org/10.1016/j.dsr2.2018.06.005, 2019.

Saavedra-Pellitero, M., Baumann, K.-H., Flores, J.-A., and Gersonde, R.: Biogeographic distribution of living coccolithophores in the Pacific sector of the Southern Ocean, Mar. Micropaleontol., 109, 1–20, https://doi.org/10.1016/j.marmicro.2014.03.003, 2014.

Saavedra-Pellitero, M., Baumann, K.-H., Bachiller-Jareno, N., Lovell, H., Vollmar, N. M., and Malinverno, E.: Mismatch between coccolithophore-based estimates of particulate inorganic carbon (PIC) concentration and satellite-derived PIC concentration in the Pacific Southern Ocean, Biogeosciences, 22, 3143–3164, https://doi.org/10.5194/bg-22-3143-2025, 2025.

Salter, I.: Seasonal variability in the persistence of dissolved environmental DNA (eDNA) in a marine system: The role of microbial nutrient limitation, PLOS ONE, 13, e0192409, https://doi.org/10.1371/journal.pone.0192409, 2018.

Salter, I., Kemp, A. E. S., Moore, C. M., Lampitt, R. S., Wolff, G. A., and Holtvoeth, J.: Diatom resting spore ecology drives enhanced carbon export from a naturally iron-fertilized bloom in the Southern Ocean, Glob. Biogeochem. Cycles, 26, https://doi.org/10.1029/2010GB003977, 2012.

Salter, I., Schiebel, R., Ziveri, P., Movellan, A., Lampitt, R., and Wolff, G. A.: Carbonate counter pump stimulated by natural iron fertilization in the Polar Frontal Zone, Nat. Geosci., 7, 885–889, https://doi.org/10.1038/ngeo2285, 2014.

Sarmiento, J. L. and Toggweiler, J. R.: A new model for the role of the oceans in determining atmospheric P CO2, Nature, 308, 621–624, https://doi.org/10.1038/308621a0, 1984.

Sarmiento, J. L., Dunne, J., Gnanadesikan, A., Key, R. M., Matsumoto, K., and Slater, R.: A new estimate of the CaCO3 to organic carbon export ratio, Glob. Biogeochem. Cycles, 16, 54-1-54–12, https://doi.org/10.1029/2002GB001919, 2002.

https://doi.org/10.5194/egusphere-2025-6347
Preprint. Discussion started: 15 January 2026

Sarmiento, J. L., Gruber, N., Brzezinski, M. A., and Dunne, J. P.: High-latitude controls of thermocline nutrients and low latitude biological productivity, Nature, 427, 56–60, https://doi.org/10.1038/nature02127, 2004.

Schmidt, K., Atkinson, A., Pond, D. W., and Ireland, L. C.: Feeding and overwintering of Antarctic krill across its major habitats: The role of sea ice cover, water depth, and phytoplankton abundance, Limnol. Oceanogr., 59, 17–36, https://doi.org/10.4319/lo.2014.59.1.0017, 2014.

Shoenfelt, E. M., Winckler, G., Lamy, F., Anderson, R. F., and Bostick, B. C.: Highly bioavailable dust-borne iron delivered to the Southern Ocean during glacial periods, Proc. Natl. Acad. Sci., 115, 11180–11185, https://doi.org/10.1073/pnas.1809755115, 2018.

Siegel, D. A., DeVries, T., Doney, S. C., and Bell, T.: Assessing the sequestration time scales of some ocean-based carbon dioxide reduction strategies, Environ. Res. Lett., 16, 104003, https://doi.org/10.1088/1748-9326/ac0be0, 2021.

Sigman, D. M., Hain, M. P., and Haug, G. H.: The polar ocean and glacial cycles in atmospheric CO2 concentration, Nature, 466, 47–55, https://doi.org/10.1038/nature09149, 2010.

Sigman, D. M., Fripiat, F., Studer, A. S., Kemeny, P. C., Martínez-García, A., Hain, M. P., Ai, X., Wang, X., Ren, H., and Haug, G. H.: The Southern Ocean during the ice ages: A review of the Antarctic surface isolation hypothesis, with comparison to the North Pacific, Quat. Sci. Rev., 254, 106732, https://doi.org/10.1016/j.quascirev.2020.106732, 2021.

Smith, A. J. R., Wotherspoon, S., Ratnarajah, L., Cutter, G. R., Macaulay, G. J., Hutton, B., King, R., Kawaguchi, S., and Cox, M. J.: Antarctic krill vertical migrations modulate seasonal carbon export, Science, 387, eadq5564, https://doi.org/10.1126/science.adq5564, 2025.

Stein, K., Timmermann, A., Kwon, E. Y., and Friedrich, T.: Timing and magnitude of Southern Ocean sea ice/carbon cycle feedbacks, Proc. Natl. Acad. Sci., 117, 4498–4504, https://doi.org/10.1073/pnas.1908670117, 2020.

Stephens, B. B. and Keeling, R. F.: The influence of Antarctic sea ice on glacial–interglacial CO2 variations, Nature, 404, 171–174, https://doi.org/10.1038/35004556, 2000.

Struve, T., Pahnke, K., Lamy, F., Wengler, M., Böning, P., and Winckler, G.: A circumpolar dust conveyor in the glacial Southern Ocean, Nat. Commun., 11, 5655, https://doi.org/10.1038/s41467-020-18858-y, 2020.

Studer, A. S., Sigman, D. M., Martínez-García, A., Benz, V., Winckler, G., Kuhn, G., Esper, O., Lamy, F., Jaccard, S. L., Wacker, L., Oleynik, S., Gersonde, R., and Haug, G. H.: Antarctic Zone nutrient conditions during the last two glacial cycles, Paleoceanography, 30, 845–862, https://doi.org/10.1002/2014PA002745, 2015.

Studer, A. S., Sigman, D. M., Martínez-García, A., Thöle, L. M., Michel, E., Jaccard, S. L., Lippold, J. A., Mazaud, A., Wang, X. T., Robinson, L. F., Adkins, J. F., and Haug, G. H.: Increased nutrient supply to the Southern Ocean during the Holocene and its implications for the pre-industrial atmospheric CO2 rise, Nat. Geosci., 11, 756–760, https://doi.org/10.1038/s41561-018-0191-8, 2018.

Tagliabue, A., Bopp, L., Roche, D. M., Bouttes, N., Dutay, J.-C., Alkama, R., Kageyama, M., Michel, E., and Paillard, D.: Quantifying the roles of ocean circulation and biogeochemistry in governing ocean carbon-13 and atmospheric carbon dioxide at the last glacial maximum, Clim. Past, 5, 695–706, https://doi.org/10.5194/cp-5-695-2009, 2009.

Thöle, L. M., Amsler, H. E., Moretti, S., Auderset, A., Gilgannon, J., Lippold, J., Vogel, H., Crosta, X., Mazaud, A., Michel, E., Martínez-García, A., and Jaccard, S. L.: Glacial-interglacial dust and export production records from the Southern Indian Ocean, Earth Planet. Sci. Lett., 525, 115716, https://doi.org/10.1016/j.epsl.2019.115716, 2019.

Toggweiler, J. R.: Variation of atmospheric CO2 by ventilation of the ocean's deepest water, Paleoceanography, 14, 571–588, https://doi.org/10.1029/1999PA900033, 1999.

https://doi.org/10.5194/egusphere-2025-6347
Preprint. Discussion started: 15 January 2026

Tréguer, P., Bowler, C., Moriceau, B., Dutkiewicz, S., Gehlen, M., Aumont, O., Bittner, L., Dugdale, R., Finkel, Z., Iudicone, D., Jahn, O., Guidi, L., Lasbleiz, M., Leblanc, K., Levy, M., and Pondaven, P.: Influence of diatom diversity on the ocean biological carbon pump, Nat. Geosci., 11, 27–37, https://doi.org/10.1038/s41561-017-0028-x, 2018.

Vollmer, T. D., Ito, T., and Lynch-Stieglitz, J.: Proxy-Based Preformed Phosphate Estimates Point to Increased Biological Pump Efficiency as Primary Cause of Last Glacial Maximum CO2 Drawdown, Paleoceanogr. Paleoclimatology, 37, e2021PA004339, https://doi.org/10.1029/2021PA004339, 2022.

Vorrath, M.-E., Müller, J., Cárdenas, P., Opel, T., Mieruch, S., Esper, O., Lembke-Jene, L., Etourneau, J., Vieth-Hillebrand, A., Lahajnar, N., Lange, C. B., Leventer, A., Evangelinos, D., Escutia, C., and Mollenhauer, G.: Deglacial and Holocene sea-ice and climate dynamics in the Bransfield Strait, northern Antarctic Peninsula, Clim. Past, 19, 1061–1079, https://doi.org/10.5194/cp-19-1061-2023, 2023.

Waelbroeck, C., Paul, A., Kucera, M., Rosell-Melé, A., Weinelt, M., Schneider, R., Mix, A. C., Abelmann, A., Armand, L., Bard, E., Barker, S., Barrows, T. T., Benway, H., Cacho, I., Chen, M.-T., Cortijo, E., Crosta, X., de Vernal, A., Dokken, T., Duprat, J., Elderfield, H., Eynaud, F., Gersonde, R., Hayes, A., Henry, M., Hillaire-Marcel, C., Huang, C.-C., Jansen, E., Juggins, S., Kallel, N., Kiefer, T., Kienast, M., Labeyrie, L., Leclaire, H., Londeix, L., Mangin, S., Matthiessen, J., Marret, F., Meland, M., Morey, A. E., Mulitza, S., Pflaumann, U., Pisias, N. G., Radi, T., Rochon, A., Rohling, E. J., Sbaffi, L., Schäfer-Neth, C., Solignac, S., Spero, H., Tachikawa, K., Turon, J.-L., and MARGO Project Members: Constraints on the magnitude and patterns of ocean cooling at the Last Glacial Maximum, Nat. Geosci., 2, 127–132, https://doi.org/10.1038/ngeo411, 2009.

Wang, X. T., Sigman, D. M., Prokopenko, M. G., Adkins, J. F., Robinson, L. F., Hines, S. K., Chai, J., Studer, A. S., Martínez-García, A., Chen, T., and Haug, G. H.: Deep-sea coral evidence for lower Southern Ocean surface nitrate concentrations during the last ice age, Proc. Natl. Acad. Sci., 114, 3352–3357, https://doi.org/10.1073/pnas.1615718114, 2017.

Warnock, J. P. and Krueger, R. E.: A record of diatom preservation from the AND-1B drillcore: The significance of taphofacies on diatom preservation, Mar. Micropaleontol., 158, 101887, https://doi.org/10.1016/j.marmicro.2020.101887, 2020.

Williams, J. R., Giering, S. L. C., Baker, C. A., Pabortsava, K., Briggs, N., East, H., Espinola, B., Blackbird, S., Le Moigne, F. a. C., Villa-Alfageme, M., Poulton, A. J., Carvalho, F., Pebody, C., Saw, K., Moore, C. M., Henson, S. A., Sanders, R., and Martin, A. P.: Inefficient transfer of diatoms through the subpolar Southern Ocean twilight zone, Nat. Geosci., 18, 72–77, https://doi.org/10.1038/s41561-024-01602-2, 2025.

Yamamoto, A., Abe-Ouchi, A., Ohgaito, R., Ito, A., and Oka, A.: Glacial CO_2 decrease and deep-water deoxygenation by iron fertilization from glaciogenic dust, Clim. Past, 15, 981–996, https://doi.org/10.5194/cp-15-981-2019, 2019.

Zúñiga, D., Sanchez-Vidal, A., Flexas, M. M., Carroll, D., Rufino, M. M., Spreen, G., Calafat, A., and Abrantes, F.: Sinking Diatom Assemblages as a Key Driver for Deep Carbon and Silicon Export in the Scotia Sea (Southern Ocean), Front. Earth Sci., 9, https://doi.org/10.3389/feart.2021.579198, 2021.